Formation of Large-Scale Structure and its Imprint on the Cosmic Microwave Background

Samuel Flender

Helsinki Institute of Physics
University of Helsinki
Finland

ACADEMIC DISSERTATION

To be presented, with the permission of the Faculty of Science of the University of Helsinki, for public criticism in the auditorium E204 of Physicum, Gustaf Hallströmin katu 2B, on the 21st of March 2014 at 12 o'clock.

Helsinki 2014

Acknowledgements

It is a pleasure to thank my supervisor Kari Enqvist for his support and motivation, and for sharing with me his wisdom about the academic world as well as about life in general. I thank Dominik Schwarz for his great ideas that lead to our first paper. I am very lucky that I got to work with Shaun Hotchkiss. He always had a lot of time for long discussions and detailed explanations. After Shaun left Helsinki, Seshadri Nadathur took his place. I learned a lot by working with both of them, and am thankful for that. I am especially thankful for Shaun's comments on an earlier version of this thesis, which improved the quality a lot. I thank the pre-examiners Hans Kristian Eriksen and Ruth Durrer for carefully examining this thesis. I am in particular thankful for Ruth's helpful comments. During my PhD studies I have had the opportunity to take some very interesting lectures and I am therefore thankful to the excellent lecturers Hannu Kurki-Suonio, Esko Keski-Vakkuri, and Jussi Väliviita. I thank Mikko Lavinto for translation of the popular abstract. Further, I wish to thank all of my colleagues, former colleagues and friends at HIP for an enjoyable working atmosphere.

I thank all of my friends in Helsinki, as well as my friends from Germany for keeping contact. I thank Hui Tang and the Kupara club for countless hours of volleyball. Finally, I am deeply grateful for the constant support and love from my family and my significant other.

Helsinki, February 2014

Samuel Flender

Abstract

One of the most important aspects of cosmology is the theory of structure formation, which describes the transition from the early, homogeneous Universe to the inhomogeneous Universe we observe today, i.e. the formation of stars, galaxies and clusters of galaxies. In this thesis, we study structure formation using the Newtonian theory of gravity within an expanding Friedmann-Robertson-Walker spacetime. We use this simple framework in order to learn for instance about the order of structure formation, which is a bottom-up evolution. Further, we introduce relativistic cosmological perturbation theory. We show that the Newtonian and relativistic descriptions of linear perturbations coincide on scales that are well inside the horizon. On larger scales however, we find differences between the two theories, in particular in the obtained linear matter power spectra.

Observations indicate that the Universe is today in a phase of accelerated expansion. In the standard model of cosmology, the ΛCDM model, the accelerated expansion is explained by the existence of dark energy in form of a cosmological constant Λ. Here, we focus on the integrated Sachs-Wolfe effect as a probe of the dynamical effects of dark energy. In particular, this effect causes an imprint of the local large-scale structure into the temperature anisotropies of the cosmic microwave background (CMB). We discuss how this effect arises in theory and how it can be measured in practice.

The statistical properties of the temperature fluctuations in the CMB can be remarkably well described within the ΛCDM model. However, on the largest angular scales some features have been found that are difficult to explain within the standard model, the so-called CMB anomalies. Here, we discuss these anomalies from a statistical point of view. We focus on one particular anomaly, the hemispherical power asymmetry, and explore its connection to the initial conditions of the Universe. In particular, this asymmetry can be related to primordial non-Gaussianity in certain inflation models.

List of Publications

The content of this thesis is based on the following research articles:

[1] S. Flender and D. Schwarz, *Newtonian versus relativistic cosmology*, Phys. Rev. D **86** (2012) 063527 [arXiv:astro-ph/1207.2035].

[2] S. Flender, S. Hotchkiss and S. Nadathur, *The stacked ISW signal of rare superstructures in ΛCDM*, JCAP **1302** (2013) 013 [arXiv:astro-ph/1212.0776].

[3] S. Flender and S. Hotchkiss, *The small scale power asymmetry in the cosmic microwave background*, JCAP **1309** (2013) 033 [arXiv:astro-ph/1307.6069].

Author's contribution

[1] I did the analytical calculations and wrote the first draft of the paper, which was edited by Prof. Schwarz.

[2] I was responsible for obtaining the stacked ISW signal from the simulated ISW maps and did part of the writing.

[3] I wrote the codes for the asymmetry analysis of the CMB map and wrote the first draft of the paper, which was edited by Dr. Hotchkiss.

Contents

Chapter 1

Introduction

Cosmology is the study of the origin, the structure, and the evolution of the Universe. Arguably the most important observation in cosmology was made in 1929 by Edwin Hubble: The Universe is expanding. This means that, as we go back in time, the Universe becomes smaller, leading ultimately to an initial state which is extremely hot and dense. This is the basic idea of the *Big Bang* theory. Today we can still observe, in every direction of the sky, the thermal radiation left over from the Big Bang, the so-called *cosmic microwave background* (CMB) radiation. Measuring and understanding this radiation gives us crucial insight into the physics of the very early Universe. The most precise measurement of the temperature anisotropies in the CMB was recently achieved by the Planck satellite. The statistical properties of these temperature fluctuations can be remarkably well described within the standard model of cosmology [4].

The small amplitude of the CMB temperature fluctuations, which is of the order of $\sim 10^{-5}$ relative to the average temperature, indicates that the Universe was extremely close to homogeneous and isotropic after the Big Bang. However, the structure of the Universe that we observe today is very inhomogeneous: we observe planets, stars and galaxies. Galaxies themselves form galaxy groups, clusters and superclusters, arranged in the form of filaments and sheets, separated by voids, leading to a particularly shaped large-scale structure referred to as the *cosmic web* [5]. The theory of *structure formation* describes the transition from the early, homogeneous Universe to the inhomogeneous Universe we observe today.

Why was the Universe so extremely close to homogeneous after the Big Bang? One possible answer to this important question is given within the theory of *inflation* (for a review see [6]): It is assumed that the very early Universe is in a phase of exponential expansion for a short period of time. This extremely fast expansion would dilute all the fluctuations in the density field, leaving the Universe very close to homogeneous. Today there are many different inflation models, and determining the most convincing one is one of the major goals in modern cosmology.

Only a small part, about 5%, of the energy density of the Universe today comes from ordinary, *baryonic* matter, i.e. matter that exists according to the standard

model of particle physics. Planets, stars and galaxies, as well as interstellar dust are all contained in this number. However, a variety of observations indicates the existence of another type of matter that we cannot see directly, but only indirectly through its gravitational effects, the so-called *dark matter*. Evidence for the existence of dark matter comes from astrophysical observations at the scales of galaxies and clusters, from CMB data, as well as from cosmological N-body simulations (for a review, see e.g. [7]). Because dark matter particles do not interact with light, they are however difficult to detect in a laboratory. Today, baryonic and dark matter together contribute 32% to the total energy content of the Universe [4]. But this is not the largest contribution.

A wide range of observations, including for instance the brightness of distant Type Ia supernovae, as well as the baryon acoustic oscillation scale in galaxy clustering, indicates that the Universe today is in a state of *accelerated expansion* (see [8] for a review). This accelerated expansion is however difficult to explain in a universe consisting only of matter, and thus leads to the idea that the Universe contains an additional form of energy with negative pressure, the so-called *dark energy*. Today, dark energy contributes 68% to the energy content of the Universe [4]. We thus live in a universe in which the largest energy contributions come from dark energy and dark matter, with only a small fraction of ordinary matter. This model of the Universe has been established as the standard model of cosmology.

The outline of this thesis is as follows. In the remainder of this chapter, we will introduce the general mathematical description of a homogeneous and isotropic universe, the basic concept of cosmic inflation, and the cosmic microwave background. In Chapter 2 we will focus on the topic of structure formation. We will discuss two different approaches to describe the structure formation process, based on perturbation theory within the Newtonian and general relativistic description of gravity. We will also discuss how this mathematical description compares to observations, i.e. galaxy correlations. In Chapter 3 we will discuss the concept of dark energy, with focus on a particular effect which causes the local large-scale structure to get imprinted into the CMB anisotropies, the *integrated Sachs-Wolfe effect*. Finally, in Chapter 4 we will discuss an interesting feature observed in the CMB sky, which might have important theoretical implications regarding the initial conditions of the Universe: the *hemispherical power asymmetry*. We will conclude with a summary in Chapter 5. This thesis is accompanied by three research articles [1-3], in which some aspects introduced in this thesis are discussed in more detail.

1.1   Standard cosmology

In this section we review the standard equations used in cosmology (see also e.g. [9]). Throughout the thesis, we will work in natural units, i.e. $\hbar = k_{\mathrm{B}} = c = 1$.

Consider a universe filled with observers that are resting with respect to each other. We refer to the time that is measured by an observer as *cosmic time t*, and the distance measured by an observer as the *physical distance* r_{phys}. If the universe is expanding, each observer will see the physical distance between two object growing with time. The *scale factor* $a(t)$ relates the physical distance measured at time t_0 to the physical distance at another time t,

$$r_{\mathrm{phys}}(t) = a(t) r_{\mathrm{phys}}(t_0), \tag{1.1}$$

with the normalization $a(t_0) = 1$. The *comoving distance* is defined as

$$r_{\mathrm{com}} = \frac{r_{\mathrm{phys}}}{a}, \tag{1.2}$$

i.e. the comoving distance remains the same at all times. The *Hubble parameter*, or *Hubble rate*, is defined as the relative speed of expansion,

$$H(t) \equiv \frac{\dot{a}(t)}{a(t)}, \tag{1.3}$$

where a dot denotes a derivative with respect to cosmic time t. Because of the expansion of space, an observer sees a distant object receding from him, with a velocity that we call the *Hubble velocity* v_{H}. *Hubble's law* relates this velocity to the physical distance to the object,

$$v_{\mathrm{H}} = H r_{\mathrm{phys}}, \tag{1.4}$$

i.e. objects that are further away recede faster.

In our Universe, we measure today a Hubble rate of $H_0 \simeq 70\,\mathrm{km/s/Mpc}$, i.e. a galaxy at a distance of $1\,\mathrm{Mpc}$ is receding from us with a velocity of about $70\,\mathrm{km/s}$. In order to work with a dimensionless quantity, one often uses the *reduced* Hubble parameter h, defined through

$$H = 100h\,\mathrm{km\,s^{-1}Mpc^{-1}}. \tag{1.5}$$

Unless otherwise stated, we will work with $h = 0.7$ throughout the thesis.

As space expands, the wavelength of photons travelling through the Universe gets stretched. The further away an observed object is, the longer it took its light to reach us, and the more its light appears *redshifted*. It is therefore common in cosmology to measure distances in terms of *redshift z*, which is defined as

$$1 + z = \frac{\lambda_{\mathrm{obs}}}{\lambda_{\mathrm{emit}}}, \tag{1.6}$$

where λ_{obs} and λ_{emit} are the wavelength of the photon at time of observation and emission, respectively. Because the wavelength scales proportionally to the scale factor, the redshift can be related to the scale factor as

$$1 + z = \frac{a_0}{a}, \tag{1.7}$$

where a_0 is the scale factor today, which we will set to 1 from now on.

1.1.1   The Friedmann-Robertson-Walker metric

If we want to describe the Universe within a mathematical model, we first need to define a measure of distance in its 4-dimensional space-time, i.e. a *metric*. The most general homogeneous and isotropic metric is the *Friedmann-Robertson-Walker* (FRW) metric [10, 11]. Its line element can be written as

$$\mathrm{d}s^2 = -dt^2 + a^2(t)\left(\frac{\mathrm{d}r^2}{1-kr^2} + r^2\mathrm{d}\theta^2 + r^2\sin^2\theta\mathrm{d}\phi^2\right), \tag{1.8}$$

where r is the comoving distance, and k denotes the curvature of space. A universe with $k = 1$ is called spatially closed, and the spatial part of the metric corresponds to a 3-sphere, S^3. In a universe with $k = -1$, a spatially open universe, the spatial part of the metric corresponds to a 3-hyperboloid, H^3. Finally, in a universe with $k = 0$, a spatially flat universe, space is described by the Euclidean metric E^3.

The defining property of General Relativity is the fundamental connection between the geometry and the content of the Universe, which is ultimately encoded in the *Einstein equation*,

$$G_{\mu\nu} = 8\pi G T_{\mu\nu}, \tag{1.9}$$

where $G_{\mu\nu}$ denotes the *Einstein tensor* and $T_{\mu\nu}$ denotes the *energy-momentum tensor* (for a review of General Relativity, see e.g. [11]). For an ideal fluid the latter is given by $T_{\mu\nu} = \mathrm{diag}(-\rho, p, p, p)$, where ρ and p are the energy density and pressure, respectively, of the fluid.

Using the Einstein tensor derived from the FRW metric and the energy-momentum tensor for an ideal fluid, the $(0, 0)$-component and the trace of the (i, j)-components of the Einstein equation give the *Friedmann equations*,

$$H^2 = \frac{8\pi G}{3}\rho - \frac{k}{a^2}, \tag{1.10}$$

$$\frac{\ddot{a}}{a} = -\frac{4\pi G}{3}(\rho + 3p). \tag{1.11}$$

The first Friedmann equation relates the speed of the expansion of space to the energy density and curvature, while the second Friedmann equation, also called *acceleration equation* or *Raychaudhuri equation*, relates the acceleration of the expansion of space to the energy density and pressure.

We define the *critical energy density* $\rho_{\mathrm{crit}} \equiv 3H^2/(8\pi G)$. The *relative energy density* is then given in terms of this quantity, $\Omega \equiv \rho/\rho_{\mathrm{crit}}$. With this definition we can rewrite the first Friedmann equation as

$$1 - \Omega(t) = -\frac{k}{a^2 H^2} \tag{1.12}$$

It is thus clear that a universe is flat if and only if it has critical energy density ($\Omega = 1$). A universe with overcritical energy density ($\Omega > 1$) is closed, a universe with undercritical energy density ($\Omega < 1$) on the other hand is open.

Another important equation is the *energy-momentum conservation equation*, or *Bianchi identity*, $\nabla_\mu T^{\mu\nu} = 0$. For an ideal fluid this gives

$$\dot{\rho} + 3H(\rho + p) = 0. \tag{1.13}$$

The *equation of state* relates the pressure of a fluid to its energy density,

$$p = w\rho, \tag{1.14}$$

where w is the *equation-of-state parameter*. Thus, we can rewrite the energy-momentum conservation as

$$\dot{\rho} + 3H(1 + w)\rho = 0. \tag{1.15}$$

For a fluid with constant w, this differential equation can be solved, yielding the scaling law for the energy density,

$$\rho \sim a^{-3(1+w)}. \tag{1.16}$$

The simplest non-trivial FRW models are one-component models. Consider the following examples:

Radiation dominated universe. The number density of photons dilutes as $\sim a^{-3}$. At the same time the wavelength of each individual photon gets stretched, so that its energy decreases as $\sim a^{-1}$. The radiation energy density thus dilutes as $\sim a^{-4}$, i.e. radiation has the equation-of-state parameter $w_r = 1/3$. A flat universe universe dominated by radiation ($\Omega = \Omega_r = 1$) expands thus as $a \sim t^{1/2}$.

Matter dominated universe. Matter dilutes as $\sim a^{-3}$ and it does not create any pressure, i.e. its equation-of-state parameter is $w_m = 0$. A flat universe dominated by matter ($\Omega = \Omega_m = 1$) expands thus as $a \sim t^{2/3}$. This model is also referred to as *Einstein-de Sitter* model.

Dark energy dominated universe. A *cosmological constant* Λ is an energy component whose energy density does not change in time. Such an energy component has $w_\Lambda = -1$, i.e. it creates negative pressure, and represents one particular dark energy model. A universe dominated by dark energy in form of a cosmological constant ($\Omega = \Omega_\Lambda = 1$) expands exponentially, $a \sim e^{Ht}$, with constant Hubble rate H. This model is also known as the *de Sitter* model.

1.1.2 The cosmological standard model

Our Universe can be described in terms of a flat FRW model with the following components [4]:

The Universe contains *baryonic matter*, i.e. matter that can be explained within the standard model of particle physics. This includes planets, stars, galaxies, as well as interstellar dust. However, this type of matter only gives a small contribution to the total energy content of the Universe, $\Omega_{bm} = 0.049$.

It has been established that the Universe contains another type of matter that we cannot see directly, but indirectly through its gravitational effects, the so-called *dark matter*. Evidence for the existence of dark matter comes from various astrophysical observations on different scales, for instance from the rotation curves and velocity dispersions of galaxies, gravitational lensing from galaxy clusters, and the so-called *Bullet Cluster*, but also from CMB data, as well as from cosmological N-body simulations (for a review, see e.g. [7]). There are many different candidates for dark matter particles from different theoretical models. Generally, if the dark matter particles are non-relativistic then we speak of *cold dark matter*, and otherwise of *hot dark matter* [12]. According to the standard model of cosmology, our Universe contains cold dark matter with a relative energy density of $\Omega_{\rm dm} = 0.268$. The total matter contribution from baryonic and dark matter is thus $\Omega_{\rm m} = \Omega_{\rm dm} + \Omega_{\rm bm} = 0.317$.

Our Universe contains relativistic particles, mainly in form of photons in the CMB radiation. There exists however also a *cosmic neutrino background*, consisting of relic neutrinos from the Big Bang. The energy density of a relativistic particle species is generally given by

$$\rho_{\rm rel}(T) = \frac{\pi^2}{30} g T^4, \tag{1.17}$$

where T is the temperature and g is the effective number of degrees of freedom of the particle species, for instance $g_\gamma = 2$ for photons and $g_\nu = 2 \cdot 7/8$ for neutrinos (see [6] for more details). Using the current CMB temperature $T_\gamma = 2.725\,{\rm K}$ [13], we find the relative energy density of photons

$$\Omega_\gamma = \frac{\rho_{\rm rel}(T_\gamma)}{\rho_{\rm c}} \simeq 5 \cdot 10^{-5}. \tag{1.18}$$

Given the temperature of the CMB, the temperature of the cosmic neutrino background can be estimated as $T_\nu = (4/11)^{1/3} T_\gamma = 1.95\,{\rm K}$ [6]. Therefore the neutrino density is

$$\Omega_\nu = \frac{7}{8} \left(\frac{4}{11}\right)^{4/3} N_{\rm eff}\,\Omega_\gamma, \tag{1.19}$$

where $N_{\rm eff}$ is the effective number of neutrino species. With the standard value $N_{\rm eff} = 3.046$ [4] we find

$$\Omega_\nu \simeq 3.5 \cdot 10^{-5}. \tag{1.20}$$

Thus, the total radiation density is

$$\Omega_{\rm r} = \Omega_\gamma + \Omega_\nu \sim 10^{-4}. \tag{1.21}$$

A wide range of observations, including for instance the brightness of distant Type Ia supernovae, as well as the baryon acoustic oscillation scale in galaxy clustering, indicates that the Universe today is in a state of *accelerated expansion*. We will discuss these observational aspects in detail in Sec. 3.1, but see also [8] for a review. The accelerated expansion can be explained by the existence of an energy component that creates negative pressure, which is generally referred to
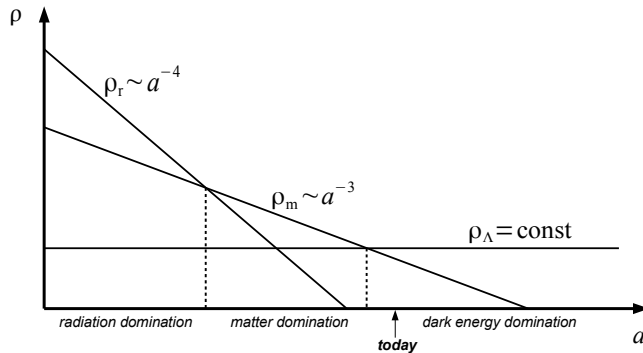
Figure 1.1: History of the Universe (not to scale). The figure illustrates the evolution of the energy densities of radiation, matter and a cosmological constant as a function of the scale factor. Due to their different scaling, there are 3 distinct eras with one component dominating.

as *dark energy*. A *cosmological constant*, usually denoted by Λ, is one particular form of dark energy whose energy density is a constant, i.e. it does not dilute with the expansion of the space. According to the standard model of cosmology, dark energy in form of a cosmological constant gives the largest contribution to the energy content of the Universe today, $\Omega_\Lambda = 0.683$.

There is no evidence for non-zero spatial curvature. Our Universe is, to an accuracy of better than a percent, spatially flat. Using Eq. (1.12), it follows that the Hubble rate at redshift z can be written as

$$H^2(z) = H_0^2 \left[\Omega_r (1+z)^4 + \Omega_m (1+z)^3 + \Omega_\Lambda \right]. \tag{1.22}$$

Because of its main components being cold dark matter and a cosmological constant Λ, the standard model of cosmology is also called the ΛCDM model.

1.1.3   History of the Universe

During the Big Bang, the Universe is extremely hot and dense. Baryonic matter and radiation are coupled tightly together, forming the *primordial plasma*. As the Universe expands, it cools down more and more. At a temperature of around $\sim 3000\,\mathrm{K}$, nuclei and electrons combine into atoms: the Universe becomes *neutral*. This process is called *recombination* or *decoupling*. The time when a photon scatters off the last free electron is called *last scattering*, and it happens at a redshift of $z \simeq 1100$. At this point, the Universe is about $380\,000$ years old. From this time on, the photons can stream freely through the Universe, giving rise to the cosmic microwave background.

Because of the different scaling of the energy components of the Universe, the known history of the Universe can be separated into three *eras* (see Fig. 1.1). Radiation dominated the first era of the Universe. But since the energy density of

radiation scales as $\sim a^{-4}$, while that of matter scales as $\sim a^{-3}$, the Universe soon changes to matter domination. At a redshift of $z \sim 3000$, radiation and matter have equally large energy contributions. This is the point of *radiation-matter equality*. Matter dominates the energy content of the Universe for most of the time after that. The next important mark is the time at which matter and dark energy have equally large energy contributions, which happens at $z \sim 0.3$. Thus, today we live in an era in which dark energy begins to dominate the energy content of the Universe.

1.1.4   Horizons

Because of the finite speed of light, there exists a finite distance that a particle could have travelled from the Big Bang until a given time. This distance is usually called the *particle horizon*. The particle horizon has thus a clear physical meaning: Any point in space is causally connected only with the region within its particle horizon. Another way to think of it is that the particle horizon separates the *observable universe* (the region within the particle horizon) from the *unobservable universe* (the region outside the particle horizon). The comoving particle horizon at a time t is given by

$$d_{\mathrm{P}}(t) \equiv \int_0^t \frac{\mathrm{d}t'}{a(t')}. \tag{1.23}$$

Another important quantity in cosmology is the so-called *Hubble horizon*. The Hubble horizon is simply given by the *Hubble length* H^{-1}, which is in our units the same as the *Hubble time*. During one Hubble time, which is the typical time scale of the expansion, light can travel one Hubble length. Throughout the rest of the thesis, we will refer to

$$d_{\mathrm{H}}(t) \equiv (aH)^{-1} \tag{1.24}$$

as the comoving *Hubble horizon*, or simply the comoving horizon. As we will see later, this horizon has an important role in the study of cosmological perturbations.

The two horizons can be related to each other. For instance, in a radiation dominated universe we have $a \sim t^{1/2}$ and therefore $d_{\mathrm{P}} = (aH)^{-1} = d_{\mathrm{H}}$. In a matter dominated universe on the other hand we have $a \sim t^{2/3}$ and thus $d_{\mathrm{P}} = 2(aH)^{-1} = 2d_{\mathrm{H}}$. From these cases it can be seen that both horizons are typically of the same order of magnitude.

1.2   Inflation

1.2.1   Motivations for inflation

There are a few important observations which the standard model of cosmology alone cannot explain. One such observation is that the primordial Universe is very close to homogeneous, which we know from the small amplitude of the CMB temperature anisotropies (of the order $\sim 10^{-5}$). This high homogeneity is however difficult to explain within the Big Bang model because regions of space that were separated by distances larger than the horizon at last scattering were not in causal

contact, making a thermalization on these large scales impossible. This problem is referred to as the *horizon problem*.

Another observation is that the Universe today appears to be very close to flat, i.e. $\Omega \simeq 1$. This is however not a stable state, i.e. if Ω is close to 1 today, its primordial value must have been much closer to 1 [6]. This is a fine-tuning problem, the so-called *flatness problem*.

Some theories predict the creation of topological defects in the early Universe due to symmetry breaking [14]. In particular, *magnetic monopoles* can be created, with an abundance that is higher than observations today allow. This is the so-called *monopole problem*.

The solution to all of these problems is given within the theory of *inflation*. It is assumed that, before the Big Bang, the Universe underwent a phase of exponential expansion for a short period of time. Inflation solves the horizon problem, because all regions of space would be causally connected before the inflationary period, the flatness problem, because the scale of a possible spatial curvature would become so large that it is practically not observable today, and the monopole problem, because all topological defects would get vastly diluted.

1.2.2 Slow-roll inflation

Here we will introduce only the basics of slow-roll inflation. For a more detailed review, see e.g. [6].

Inflation is a period of exponential expansion, i.e. $a(t) \sim e^{Ht}$, with an almost constant Hubble parameter $H \simeq \text{const}$. Using the *reduced Planck mass*,

$$M_{\text{Pl}}^2 \equiv 1/(8\pi G),\tag{1.25}$$

the Friedmann equation (1.10) can be rewritten as

$$\rho = 3M_{\text{Pl}}^2 H^2.\tag{1.26}$$

Thus, from near constancy of the Hubble parameter it follows that the energy density during inflation is nearly constant. From Eq. (1.16) it follows that $w \simeq -1$. All of these argumentation steps are invertible, i.e. inflation happens if and only if $w \simeq -1$.

Inflation can be explained with the existence of a scalar field, the *inflaton* ϕ. Let its Lagrangian be

$$\mathcal{L} = -\frac{1}{2}\phi^{,\mu}\phi_{,\mu} - V(\phi),\tag{1.27}$$

with some potential $V(\phi)$. The energy density and pressure are then given by

$$\rho = \frac{1}{2}\dot{\phi}^2 + V(\phi),\tag{1.28}$$

$$p = \frac{1}{2}\dot{\phi}^2 - V(\phi).\tag{1.29}$$

If the potential energy dominates over the kinetic energy, i.e. $\frac{1}{2}\dot{\phi}^2 \ll V(\phi)$, it follows that $w = p/\rho \simeq -1$, so that inflation happens. This limit is the *slow-roll approximation*, and the type of inflation is called *slow-roll inflation*.
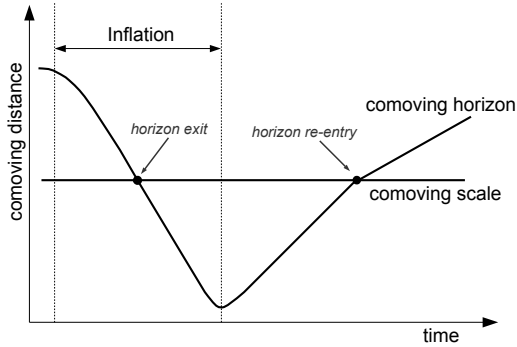
Figure 1.2: Schematic evolution of the horizon (not to scale). A given comoving scale leaves the horizon during inflation and re-enters the horizon much later, when the Universe is radiation- or matter dominated.

In the context of slow-roll inflation one usually defines the *slow-roll parameters*,

$$\epsilon \quad \equiv \quad \frac{M_{\mathrm{Pl}}^2}{2} \left(\frac{V'}{V} \right)^2, \tag{1.30}$$

$$\eta \quad \equiv \quad M_{\mathrm{Pl}}^2 \frac{V''}{V}, \tag{1.31}$$

where a prime in this context denotes a derivative with respect to the inflaton field ϕ. The parameter ϵ describes the slope of the potential V, which has to be small enough so that the kinetic energy of the inflaton is negligible compared to its potential energy. The parameter η on the other hand describes the curvature of the potential and thus determines how long slow-roll inflation will last.

1.2.3   Evolution of the horizon

During inflation the Universe is expanding as $a \sim e^{Ht}$, with a nearly constant Hubble rate H. The comoving horizon is thus shrinking, $d_{\mathrm{H}} \sim e^{-Ht}$, i.e. during inflation all scales leave the horizon. During radiation domination we have

$$a \sim t^{1/2} \Rightarrow H = \frac{1}{2t} \Rightarrow d_{\mathrm{H}} \sim t^{1/2}, \tag{1.32}$$

and during matter domination

$$a \sim t^{2/3} \Rightarrow H = \frac{2}{3t} \Rightarrow d_{\mathrm{H}} \sim t^{1/3}. \tag{1.33}$$

Hence, the scales that leave the horizon during inflation will re-enter the horizon later, during radiation- or matter domination (see Fig. 1.2). Scales leaving the horizon last will re-enter first, and vice versa.

1.3   The cosmic microwave background

The cosmic microwave background is created at the time of last scattering, when photons start propagating freely through the Universe. Due to the redshift, we measure this radiation today in the microwave range. The CMB radiation has a black-body spectrum corresponding to a temperature of $2.725\,\mathrm{K}$ [13], and is almost perfectly isotropic, with small temperature anisotropies which are of the order of $\sim 10^{-5}$ relative to the average temperature (see Fig. 1.3). The primary source of these anisotropies is the existence of small density inhomogeneities in the primordial Universe: CMB photons that were in a slightly overdense region at the time of last scattering are slightly colder because they lost some energy climbing out of the potential well. Similarly, CMB photons from an underdense region are slightly hotter.

1.3.1   Spherical harmonics expansion

Because the last scattering surface can be considered as the surface of a sphere surrounding us, the CMB temperature anisotropy $\delta T(\mathbf{n})$, measured in a direction $\mathbf{n}$, can be expanded in terms of *spherical harmonics* $Y_{\ell m}$,

$$\delta T(\mathbf{n}) = \sum_{\ell,m} a_{\ell m} Y_{\ell m}(\mathbf{n}). \tag{1.34}$$

The spherical harmonics $Y_{\ell m}$ form an orthonormal basis on the surface of a sphere,

$$\int \mathrm{d}\Omega\, Y_{\ell m} Y_{\ell' m'}^* = \delta_{\ell \ell'} \delta_{mm'}, \tag{1.35}$$

and satisfy the following addition theorem:

$$\sum_m Y_{\ell m}(\mathbf{n}) Y_{\ell m}^*(\mathbf{n}') = \frac{2\ell + 1}{4\pi} P_\ell(\mathbf{n} \cdot \mathbf{n}'), \tag{1.36}$$

where P_ℓ are the Legendre-polynomials.

The coefficients $a_{\ell m}$ are random variables drawn from a Gaussian distribution with zero mean. The coefficients are *statistically independent*, so that the correlation of $a_{\ell m}$ with different ℓ and m vanishes,

$$\langle a_{\ell m} a_{\ell' m'}^* \rangle \sim \delta_{\ell \ell'} \delta_{mm'}, \tag{1.37}$$

where $\langle \cdot \rangle$ denotes the *ensemble* average. Furthermore, inflation predicts the Universe to be statistically isotropic, so that the constant of proportionality only depends on ℓ, not m,

$$\langle a_{\ell m} a_{\ell' m'}^* \rangle = C_\ell \delta_{\ell \ell'} \delta_{mm'}, \tag{1.38}$$

where C_ℓ is the *angular power* at the multipole ℓ.

The *two-point correlation function* $C(\theta)$ is defined as

$$C(\theta) = \langle \delta T(\mathbf{n}) \delta T^*(\mathbf{n}') \rangle \ , \quad \cos\theta = \mathbf{n} \cdot \mathbf{n}'. \tag{1.39}$$
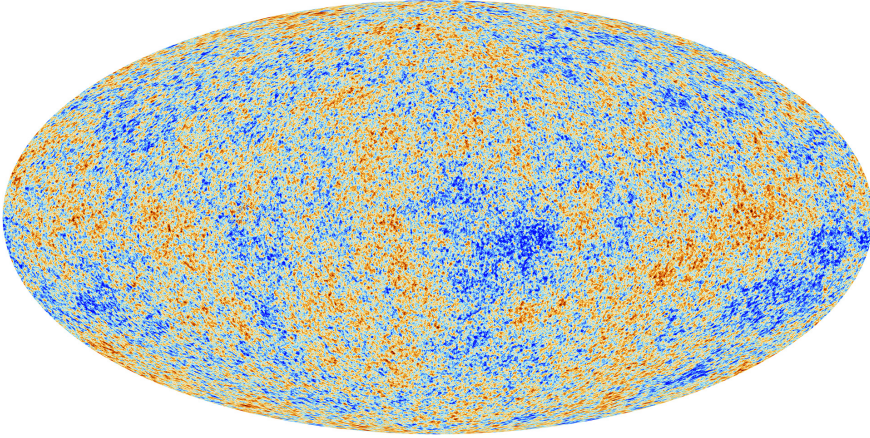
Figure 1.3: Temperature map of the cosmic microwave background, as measured by the Planck satellite. The color scale ranges from $-300\,\mu$K (blue) to $+300\,\mu$K (red), relative to the CMB average temperature. (Image credit: ESA/Planck)
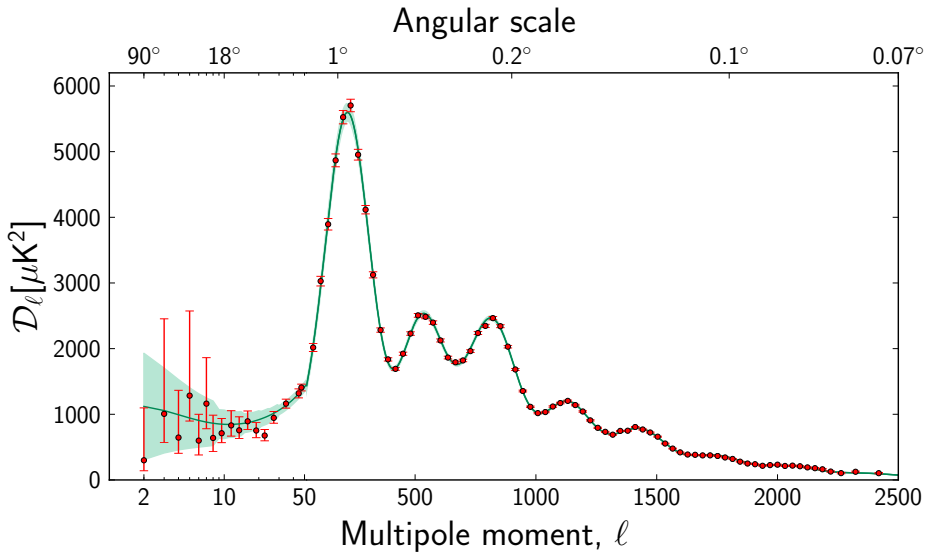
Figure 1.4: Angular power spectrum $\mathcal{D}_\ell = \ell(\ell+1)C_\ell/(2\pi)$ of the CMB, as measured by the Planck satellite. The red points correspond to the data, while the green line shows the best-fit ΛCDM model. The shaded green area indicates cosmic variance. The ℓ-axis is logarithmic up to $\ell = 50$, and linear from $\ell = 50$ onwards. Plot taken from [15].

Using Eqs. (1.38) and (1.36), we can derive a relation between the two-point correlation function and the power spectrum,

$$C(\theta) = \langle \delta T(\mathbf{n}) \delta T^*(\mathbf{n}') \rangle = \sum_{\ell,m} \sum_{\ell',m'} \langle a_{\ell m} a_{\ell'm'}^* \rangle Y_{\ell m}(\mathbf{n}) Y_{\ell'm'}^*(\mathbf{n}') \quad (1.40)$$

$$= \frac{1}{4\pi} \sum_{\ell} (2\ell + 1) C_\ell P_\ell(\cos\theta). \quad (1.41)$$

Thus, the two-point correlation function and the angular power spectrum contain the same statistical information.

From Eq. (1.38) it follows that the angular power spectrum can be expressed as $C_\ell = \langle |a_{\ell m}|^2 \rangle$. In practice, the *ensemble* average in that equation cannot be measured, because we only observe *one* sky, i.e. one realization of the set of $a_{\ell m}$ coefficients. The best we can do is to find an *estimator* $\hat{C}_\ell$ for the power spectrum. For example, we can take the average of all measured $a_{\ell m}$ in our sky, the *sky average*,

$$\hat{C}_\ell = \frac{1}{2\ell + 1} \sum_{m=-\ell}^{\ell} |a_{\ell m}|^2. \quad (1.42)$$

The variance (mean square error) of this estimator is then given by [16]

$$\mathrm{Var}(\hat{\mathrm{C}}_\ell) = \frac{2}{2\ell + 1} \hat{\mathrm{C}}_\ell^2. \quad (1.43)$$

This error is the *cosmic variance*. The cosmic variance increases at lower multipoles because less statistical information about large-scale correlations is available from only one sky. The estimation of the angular power with this estimator is thus much more precise on small angular scales.

1.3.2   The angular power spectrum

In this section we will discuss the most important features in the angular power spectrum of the measured CMB (see Fig. 1.4). For a more detailed discussion, see e.g. [16, 6].

A characteristic feature in the CMB power spectrum is the occurrence of several peaks, at an angular scale of $1°$ and smaller. These are the so-called *acoustic peaks*, created as follows. During radiation domination, photon pressure prevents the gravitational collapse of baryonic matter perturbations, leading to the creation of longitudinal (acoustic) oscillations in the photon-baryon fluid called the *baryon-acoustic oscillations*. After decoupling, these oscillations become imprinted into the CMB. The physical scale of these oscillations is determined by the distance that sound waves can travel until the time of last scattering, the so-called *sound horizon*. We see the first acoustic peak at an angular scale of $\simeq 1°$ because this is the angle subtended by the sound horizon. In fact, if the geometry of space was not flat, then we would see the first acoustic peak at a different angle. Therefore, the position of the first acoustic peak is evidence that the Universe is flat [16]. The other acoustic peaks at smaller angular scales correspond to higher oscillation

modes. On much smaller angular scales however, photons can diffuse from hot regions to cold regions in the photon-baryon plasma. This leads to a damping of the higher acoustic peaks, the so-called *diffusion damping* or *Silk damping*.

The horizon at the time of last scattering corresponds to a multipole of $\ell \simeq 70$. Perturbations at multipoles below that are thus super-horizon perturbations at the time of last scattering. The CMB temperature fluctuations at these multipoles are directly related to the perturbations in the gravitational field ϕ,

$$\frac{\delta T}{T} \simeq \frac{1}{3}\phi. \tag{1.44}$$

This is the so-called *Sachs-Wolfe* effect. Scale-invariance of the primordial perturbations causes constancy of $\ell(\ell+1)C_\ell$ at the low multipoles, which is referred to as the *Sachs-Wolfe plateau*. In order to make the Sachs-Wolfe plateau more visible, one often plots the angular power in terms of the quantity $\mathcal{D}_\ell \equiv \ell(\ell+1)C_\ell/(2\pi)$, with a logarithmic ℓ-axis.

Decay of the gravitational potential ϕ causes secondary anisotropies in the CMB, i.e. anisotropies that are not created at the time of last scattering, but instead during the journey of the CMB photons from the last scattering surface to us. These secondary anisotropies are referred to as the *integrated Sachs-Wolfe* (ISW) effect [17]. The gravitational potential decays during radiation domination and during dark energy domination. Therefore, the ISW effect occurs twice, once directly after last scattering, when the Universe is not yet completely matter dominated, and once in the late Universe, when dark energy begins to dominate. There is thus an *early* and a *late* ISW effect. The late ISW effect causes the slope in the Sachs-Wolfe plateau at multipoles $\ell \lesssim 10$.

Because the late ISW effect reflects the dynamical effects of dark energy, its detection is important for our understanding of the nature of dark energy, and can be used to test the ΛCDM model. Unfortunately, the ISW signal cannot be measured from the CMB angular power spectrum directly because of large cosmic variance at the low multipoles. It can however be extracted from the CMB using other methods, as we will describe in detail later, in Sec. 3.3.

Chapter 2

Structure formation

After inflation ends, the Universe is almost perfectly homogeneous, with small fluctuations in the curvature field of the order of $\sim 10^{-5}$. However, the structure of the Universe we observe today is very inhomogeneous: we observe galaxies, which themselves form galaxy groups, clusters and superclusters, arranged in form of filaments and sheets, separated by voids (see Fig. 2.1). This leads to a particularly shaped large-scale structure of the Universe referred to as the *cosmic web* [5].

The transition from the early, homogeneous Universe to the inhomogeneous Universe we observe today is described within the theory of *structure formation*. The mathematical framework to describe this process accurately, at least in the linear regime, is relativistic cosmological perturbation theory, in which we consider perturbations in the FRW metric tensor and the energy-momentum tensor. Another, much simpler, approach is based on perturbations described within Newton's theory of gravity on top of an expanding, homogenous and isotropic FRW background. We will study both approaches in detail in the following sections.

2.1 Perturbations in Newtonian cosmology

In the Newtonian description of structure formation we consider the Newtonian equations of motion within an expanding FRW universe, for which we know the evolution of the scale factor a and the Hubble parameter H from the Friedmann equations. In this section we will consider a universe filled only with pressureless matter, corresponding to cold dark matter, i.e. a universe with $\Omega = \Omega_{\mathrm{m}} = 1$ (Einstein-de Sitter model). This is a simplification compared to the ΛCDM model, where we also have to take into account the presence of radiation, baryonic matter and a cosmological constant. However, it can be justified with the fact that the Universe was matter dominated during most of the time of the structure formation process. As will be shown, the effect of the radiation dominated era on structure formation can be taken into account with the use of transfer functions. For a more detailed review of cosmological perturbations within Newtonian theory, see also [18].

In addition to cosmic time t, we introduce *conformal time* τ, defined through
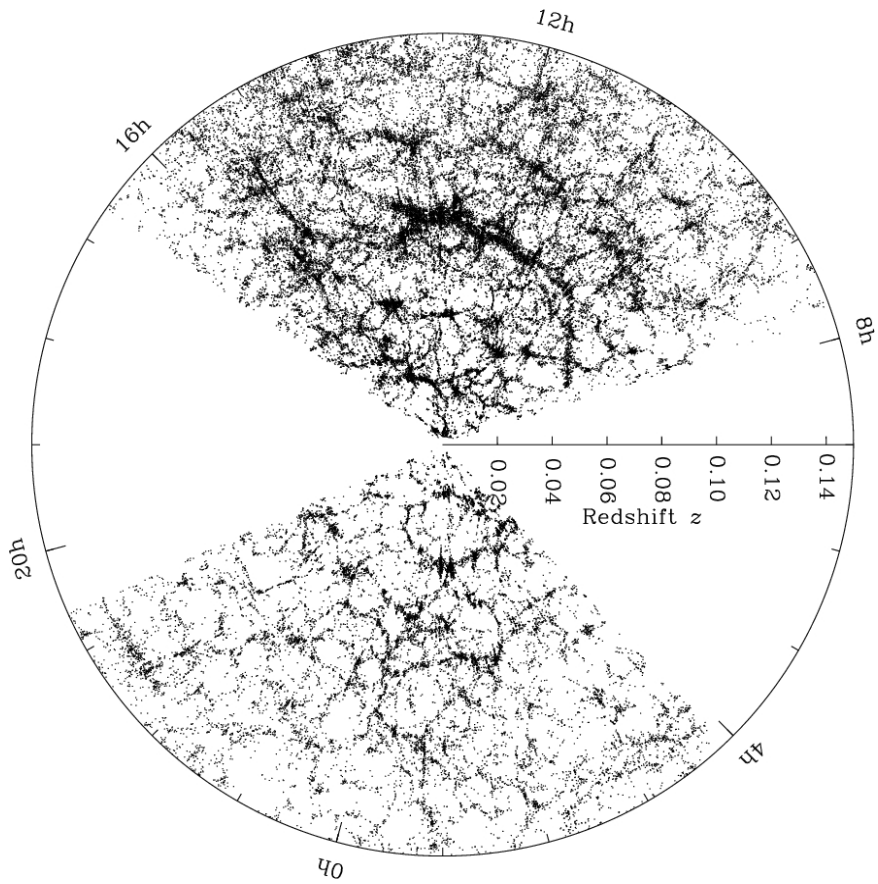
Figure 2.1: Large scale structure of the Universe. The map shows the distribution of galaxies around the Milky Way, each dot representing one galaxy. Image credit: SDSS project.

$dt = ad\tau$. A prime denotes a partial derivative with respect to conformal time. Further we define, in addition to the Hubble parameter $H = \dot{a}/a$, the conformal Hubble parameter $\mathcal{H} = a'/a$. The *absolute velocity* $\mathbf{u}$ of a particle in an expanding FRW universe is given by

$$\mathbf{u} = \frac{d\mathbf{r}}{dt} = H\mathbf{r} + \mathbf{v} = \mathbf{v}_H + \mathbf{v}, \tag{2.1}$$

where $\mathbf{v}_H$ is the Hubble velocity, and $\mathbf{v}$ is the *peculiar velocity*, which measures the particle's velocity relative to the Hubble expansion.

2.1.1 Evolution equations

In order to understand the process of structure formation, we need to know the time evolution of three fields, the matter density field ρ, the gravitational potential field Φ, and velocity field $\mathbf{u}$. We approximate these fields as a combination of a background part and a small perturbation,

$$\rho = \bar{\rho} + \delta\rho = \bar{\rho}(1 + \delta), \tag{2.2}$$
$$\Phi = \bar{\Phi} + \phi, \tag{2.3}$$
$$\mathbf{u} = \mathbf{v}_H + \mathbf{v}, \tag{2.4}$$

where we defined the *density contrast* $\delta \equiv \delta\rho/\bar{\rho}$. Here, we will consider first order perturbation theory, i.e. products of two perturbations are considered negligibly small. Note that, because of spatial symmetry of the FRW background, the background fields are functions of time only, while the perturbations are functions of time and space.

The relevant equations are the *continuity equation*, the *Poisson equation*, and the *Euler equation*. Using comoving coordinates and conformal time, those can be written as [18]

$$\rho' + 3\mathcal{H}\rho + \nabla \cdot (\rho\mathbf{v}) = 0, \tag{2.5}$$
$$\nabla^2\Phi = 4\pi Ga^2\rho, \tag{2.6}$$
$$\mathcal{H}'\mathbf{x} + \mathbf{v}' + \mathcal{H}\mathbf{v} + \mathbf{v} \cdot \nabla\mathbf{v} = -\nabla\Phi. \tag{2.7}$$

In the background order, this system of equations reduces to

$$\bar{\rho}' + 3\mathcal{H}\bar{\rho} = 0, \tag{2.8}$$
$$\nabla^2\bar{\Phi} = 4\pi Ga^2\bar{\rho}, \tag{2.9}$$
$$\mathcal{H}'\mathbf{x} = -\nabla\bar{\Phi}. \tag{2.10}$$

The first two of these equations give the evolution of the background matter density, $\bar{\rho} \sim a^{-3}$, as well as the background potential at a point $\mathbf{x}$ relative to a reference point $\mathbf{x}_0$, $\bar{\Phi} = (4/3)\pi Ga^2\bar{\rho}(\mathbf{x} - \mathbf{x}_0)^2$. From the divergence of Eq. (2.10) we find $\mathcal{H}' = -\frac{4}{3}\pi Ga^2\bar{\rho}$, i.e. the Raychaudhuri equation for $p = 0$.

In linear order the set of equations reads:

$$\delta' + \nabla \cdot \mathbf{v} = 0, \tag{2.11}$$

$$\nabla^2 \phi = \frac{3}{2}\mathcal{H}^2 \delta, \tag{2.12}$$

$$\mathbf{v}' + \mathcal{H}\mathbf{v} = -\nabla\phi, \tag{2.13}$$

where we used the Friedmann equation, $\mathcal{H}^2 = (8/3)\pi G \bar{\rho} a^2$, in order to replace the right hand side of the Poisson equation.

Transforming into Fourier (momentum) space, we find:

$$\delta_k' + i\mathbf{k} \cdot \mathbf{v}_k = 0, \tag{2.14}$$

$$-k^2 \phi_k = \frac{3}{2}\mathcal{H}^2 \delta_k, \tag{2.15}$$

$$\mathbf{v}_k' + \mathcal{H}\mathbf{v}_k = -i\mathbf{k}\phi_k. \tag{2.16}$$

The growing solutions are then given by:

$$\phi_k = \text{const}, \tag{2.17}$$

$$\delta_k = -\frac{2}{3}\frac{k^2}{\mathcal{H}^2}\phi, \tag{2.18}$$

$$\mathbf{v}_k = -\frac{2}{3}i\frac{\mathbf{k}}{\mathcal{H}}\phi. \tag{2.19}$$

2.1.2 Statistics of Gaussian perturbations

Before discussing the evolution of perturbations in the Universe, we first need to understand the statistical properties of Gaussian perturbations. Consider a perturbation field $g(\mathbf{x})$ with Fourier modes given by

$$g(\mathbf{k}) = \int \frac{\mathrm{d}^3 x}{(2\pi)^{3/2}} g(\mathbf{x}) e^{-i\mathbf{k}\cdot\mathbf{x}}. \tag{2.20}$$

A Gaussian perturbation field $g(\mathbf{x})$ is a perturbation with a Gaussian probability distribution function, i.e. the probability of finding the value g for the field $g(\mathbf{x})$ is given by

$$\text{Prob}(g)\mathrm{d}g = \frac{1}{\sqrt{2\pi}\sigma_g} \exp(-\frac{g^2}{2\sigma_g^2})\mathrm{d}g, \tag{2.21}$$

where σ_g^2 is the variance of the field $g(\mathbf{x})$.

Homogeneity of the field $g(\mathbf{x})$ implies that its Fourier modes are uncorrelated, i.e.

$$\langle g(\mathbf{k})g^*(\mathbf{k}')\rangle \sim \delta(\mathbf{k} - \mathbf{k}'), \tag{2.22}$$

where $\langle \cdot \rangle$ denotes the *ensemble* average. If we further assume isotropy, it follows that the constant of proportionality depends only on the absolute value of $\mathbf{k}$, not its direction. We can thus write

$$\langle g(\mathbf{k})g^*(\mathbf{k}')\rangle = P(k)\delta(\mathbf{k} - \mathbf{k}'), \tag{2.23}$$

where we introduced the *power spectrum* $P(k)$. For Gaussian perturbations, all of the statistical information is encoded in the power spectrum.

Another important quantity is the *two-point correlation function*,

$$\xi(\mathbf{x}, \mathbf{x}') \equiv \langle g(\mathbf{x})g^*(\mathbf{x}')\rangle. \tag{2.24}$$

It is related to the power spectrum as

$$
\begin{aligned}
\langle g(\mathbf{x})g^*(\mathbf{x}')\rangle &= \int \frac{d^3k}{(2\pi)^{3/2}} e^{i\mathbf{k}\cdot\mathbf{x}} \int \frac{d^3k'}{(2\pi)^{3/2}} e^{i\mathbf{k}'\cdot\mathbf{x}'} \langle g(\mathbf{k})g^*(\mathbf{k}')\rangle \\
&= \int_0^\infty \frac{dk}{k} \frac{\sin(kr)}{kr} \frac{k^3}{2\pi^2} P(k),
\end{aligned} \tag{2.25}
$$

where $r \equiv |\mathbf{x} - \mathbf{x}'|$ is the distance between the two points $\mathbf{x}$ and $\mathbf{x}'$. The dimensionless (band) power spectrum is defined as

$$\mathcal{P}(k) \equiv \frac{k^3}{2\pi^2} P(k). \tag{2.26}$$

Taking the limit $r \to 0$ of Eq. (2.25), we find a relation between the variance of the field g and the band power,

$$\sigma_g^2 = \langle |g(\mathbf{x})|^2 \rangle = \int_0^\infty \frac{dk}{k} \mathcal{P}(k). \tag{2.27}$$

A *power-law* spectrum has the form

$$\mathcal{P}(k) = A^2 \left(\frac{k}{k_{\text{pivot}}}\right)^{n_s - 1}, \tag{2.28}$$

where A is the power amplitude at the reference scale k_{pivot}, and the *spectral index* n_s describes the scale-dependence of the power; $n_s < 1$ describes a spectrum with more power on large scales, $n_s > 1$ a spectrum with more power on small scales. For $n_s = 1$ the power is the same on all scales. This spectrum is also called the *Harrison-Zel'dovich* spectrum.

Note that for a Harrison-Zel'dovich spectrum the variance $\langle |g(\mathbf{x})|^2 \rangle$ is logarithmically divergent, both at large scales ($k \to 0$) and at small scales ($k \to \infty$). One therefore usually introduces an infrared-cutoff and an ultraviolet-cutoff in order to make the integral finite. The ultraviolet divergence can alternatively be removed by the introduction of a *window function* $W(k, R_F)$, which filters out fluctuations at scales much smaller than the filter scale R_F. The *filtered* variance is then

$$\sigma_{g,R_F}^2 = \int_0^\infty \frac{dk}{k} \mathcal{P}(k) W^2(k, R_F). \tag{2.29}$$

2.1.3 Matter power spectrum

In the simplest models of inflation, perturbations in the inflaton field, $\delta\phi$, generate the primordial curvature perturbations ζ, which are the important seeds for structure formation. In slow-roll inflation, the curvature perturbation field is predicted

to be highly Gaussian, with an almost scale-invariant power spectrum [19]. In particular, the spectral index can be related to the slow-roll parameters (defined in Sec. 1.2.2) as [6]

$$n_{\rm s} - 1 = -6\epsilon + 2\eta, \tag{2.30}$$

i.e. the smallness of the slow-roll parameters implies closeness to unity of the spectral index. In fact, the Planck data gives a spectral index very close to one, $n_{\rm s} = 0.9616 \pm 0.0094$. The amplitude is determined to be $A^2 = (2.23 \pm 0.16) \cdot 10^{-9}$ at the reference scale $k_{\rm pivot} = 0.05\,{\rm Mpc}^{-1}$ [4].

In a matter dominated universe, the metric potential Φ (which can be identified as the gravitational potential) is related to the curvature perturbation ζ as [20]

$$\Phi = -\frac{3}{5}\,\zeta. \tag{2.31}$$

We thus find for the power spectrum of the gravitational potential

$$\mathcal{P}_\phi(k) = \frac{9}{25}A^2\left(\frac{k}{k_{\rm pivot}}\right)^{n_{\rm s}-1}, \tag{2.32}$$

and, using Eq. (2.18), for the density contrast

$$\mathcal{P}_\delta(k) = \frac{4}{25}A^2\frac{k^4}{\mathcal{H}^4}\left(\frac{k}{k_{\rm pivot}}\right)^{n_{\rm s}-1}. \tag{2.33}$$

This is the linear matter power spectrum in a universe which is always matter dominated, i.e. an Einstein-de Sitter universe. Our Universe however was not always matter dominated. We thus have to take into account the effect of the radiation dominated era on the power spectrum.

2.1.4   Transfer function

During radiation domination, the evolution equations for the perturbations are as above, Eqs. (2.11)-(2.13), with the only change appearing in form of a pressure gradient in the Euler equation:

$$\delta' + \nabla \cdot \mathbf{v} = 0, \tag{2.34}$$

$$\nabla^2\phi = 4\pi G\bar{\rho}_{\rm m}a^2\delta, \tag{2.35}$$

$$\mathbf{v}' + \mathcal{H}\mathbf{v} = -\nabla\phi - \frac{1}{\bar{\rho}}\nabla\delta p. \tag{2.36}$$

Here, $\bar{\rho} = \bar{\rho}_{\rm m} + \bar{\rho}_{\rm r}$ is the total energy density from matter and radiation, and δp is the pressure perturbation. It can be shown that for isentropic perturbations, i.e. perturbations with vanishing entropy gradient, the pressure gradient can be transformed into a density gradient, $\frac{1}{\bar{\rho}}\nabla\delta p = c_{\rm s}^2\nabla\delta$, where $c_{\rm s}$ is the *speed of sound*, defined as $c_{\rm s}^2 \equiv {\rm d}\bar{p}/{\rm d}\bar{\rho}$ [18].

Taking the time derivate of the continuity equation and the gradient of the Euler equation, replacing $\nabla^2\phi$ using the Poisson equation, we find the *Jeans equation*,

$$\delta'' + \mathcal{H}\delta' = 4\pi G\bar{\rho}_{\rm m}a^2\delta + \nabla^2 c_{\rm s}^2\delta. \tag{2.37}$$

In momentum space the Jeans equation reads

$$\delta'' + \mathcal{H}\delta' = (k_J^2 - k^2)c_s^2\delta, \qquad (2.38)$$

where we have introduced the *Jeans wavenumber*

$$k_J \equiv c_s^{-1}\sqrt{4\pi G\bar{\rho}_m a^2}. \qquad (2.39)$$

There is thus a characteristic scale, the Jeans scale k_J^{-1}. On scales much smaller than the Jeans scale ($k \gg k_J$), baryonic matter perturbations are oscillating, with an oscillation amplitude that is decaying due to Hubble friction. On scales much larger than the Jeans scale ($k \ll k_J$), the baryonic matter perturbations grow as $\delta \sim \ln a$. For dark matter perturbations, the situation is a bit different because dark matter particles do not interact with light, i.e. they are not affected by the photon pressure. Dark matter perturbations grow generally as $\delta \sim \ln a$ during radiation domination. This is however much slower than the growth rate during matter domination ($\delta \sim a$). Thus, the growth of perturbations is suppressed during radiation domination.

One important implication of Eq. (2.33) and $n_s \simeq 1$ is that the amplitude of the matter perturbations at horizon entry ($k/\mathcal{H} = 1$) is approximately the same for all scales. This means that the amplitude of the perturbation today is determined by the growth during the whole time from horizon entry until today. There is thus an important difference between scales that enter the horizon before the radiation-matter equality and after: Perturbations on scales entering before the equality will experience a suppression in growth, while perturbations on scales entering after the equality will not. In other words, perturbations on scales $k^{-1} < k_{eq}^{-1}$ will be suppressed, where the *equality scale* $k_{eq}^{-1} \simeq 70\,\text{Mpc}$ is the scale that enters the horizon during radiation-matter equality.

The suppression of growth leads to a suppression of power at scales $k^{-1} < k_{eq}^{-1}$, which can be absorbed into the matter power spectrum by including a *transfer function $T(k)$*. In [21] several analytical expressions for the transfer function were derived, corresponding to different dark matter models. For cold dark matter perturbations, the transfer function can be expressed as

$$T(k) = \frac{\ln(1 + 2.34q)}{2.34q}[1 + 3.89q + (16.1q)^2 + (5.46q)^3 + (6.71q)^4]^{-1/4}, \qquad (2.40)$$

where $q \equiv k/(\Gamma h\text{Mpc}^{-1})$, and Γ is the *shape parameter*,

$$\Gamma \equiv \Omega_{tot}h\exp(-\Omega_{bm} - \sqrt{2h}\frac{\Omega_{bm}}{\Omega_{tot}}), \qquad (2.41)$$

where Ω_{tot} and Ω_{bm} are the total and baryonic relative energy densities, respectively, of the Universe today. We will use this transfer function throughout the rest of this thesis (see Fig. 2.2 for a plot). Including the transfer function, the power spectrum reads

$$\mathcal{P}_\delta(k) = \frac{4}{25}A^2T^2(k)\frac{k^4}{\mathcal{H}^4}\left(\frac{k}{k_{pivot}}\right)^{n_s-1}. \qquad (2.42)$$
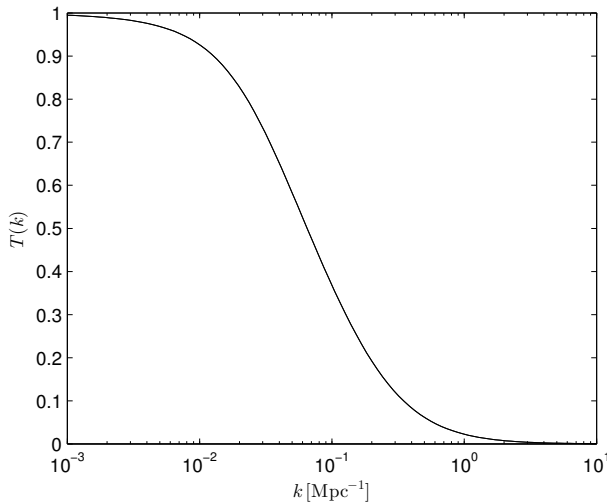
Figure 2.2:   The *BBKS* transfer function $T(k)$, with parameters $\Omega_{\text{tot}} = 1$, $\Omega_{\text{bm}} = 0.049$, and $h = 0.7$. The transfer function accounts for the suppression of power at scales $k^{-1} < k_{\text{eq}}^{-1} \simeq 70\,\text{Mpc}$.

This is our final result for the linear matter power spectrum in Newtonian theory.

Note that after decoupling dark matter perturbations are much larger than baryonic matter perturbation because dark matter perturbations already start growing during radiation domination. Consequently, the baryons fall into the dark matter potential wells, which boosts the growth of their perturbations. Thus, the presence of dark matter fastens up the structure formation process.

2.1.5   Non-linear regime

Perturbation theory can be applied as long as the perturbations remain small. From the spherical collapse model we know that linear theory breaks down when the density contrast reaches unity, i.e. the density becomes locally twice as large as the background value [6, 22]. At this point the system collapses and viralizes into a gravitationally bound object, where its kinetic energy prevents further collapse.

The bound structures formed from cold dark matter are the so-called dark matter *halos* [23]. Baryonic matter falls into these dark matter halos and cools, leading to the formation of galaxies in the centres of the dark matter halos, the so-called *central galaxies* [24]. With time, dark matter halos can merge and form bigger halos, containing more galaxies. This leads to the formation of galaxy groups and clusters.

We can learn about the order of structure formation by analyzing when the theoretical band power, given in Eq. (2.42), becomes unity on a given scale (see also Fig. 2.3). For instance, perturbations on galactic scales ($\sim 1\,\text{Mpc}$) become nonlinear at $z \sim 7$. This means that we should see the first galaxies roughly at
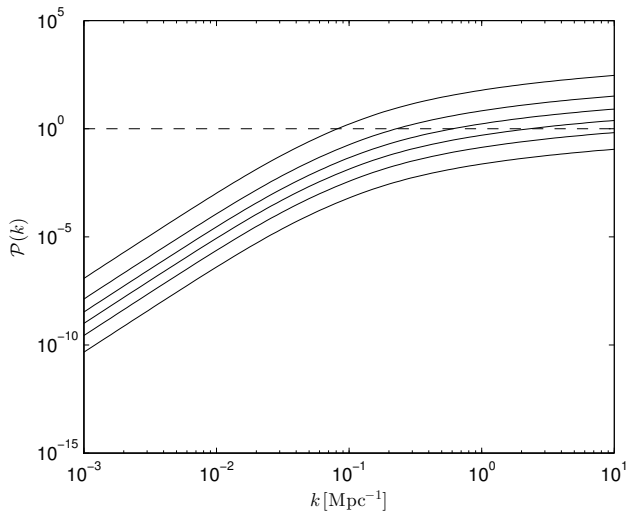
Figure 2.3: Dimensionless matter power spectrum $\mathcal{P}(k)$ at different redshifts, from bottom to top, $z = 50, 20, 10, 5, 2, 0$. Linear theory is valid until $\mathcal{P}(k) \sim 1$ (dashed line).

that redshift. In fact, the furthest confirmed galaxy has a redshift of $z = 7.51$ [25]. Perturbations on cluster scales ($\sim 10\,\mathrm{Mpc}$) become nonlinear at redshift $z \sim 0.3$. This is why we can see clusters of galaxies for instance in the SDSS (see Fig. 2.1). Perturbations on even larger scales are still linear today. In an Einstein-de Sitter model, perturbations on those scales would become nonlinear some time in the future. In our Universe however they will never become nonlinear because of the presence of dark energy, which causes the density contrast to freeze out, as we will show in Sec. 3.2. To summarize, structures on small scales (e.g. galaxies) form before structures on large scales (e.g. clusters). This scenario of structure formation is the so-called *bottom-up* scenario.

The breakdown of perturbation theory at $\delta \sim 1$ prevents us from understanding the nonlinear formation of structure analytically. This motivates the use of cosmological N-body simulations, which work as follows. At an initial redshift (typically $z = 100$, where perturbations on all scales are still in the linear regime), 'particles' are distributed in a simulation box, each of which represents a heavy dark matter clump. Then the potential field caused by the current matter distribution is calculated with the Poisson equation, and particles are moved according to the Euler equation. This process is repeated until $z = 0$, providing a complete nonlinear picture of structure formation. Note however that these simulations use Newtonian equations of motion. We will discuss the validity of the Newtonian equations later, in Sec. 2.2.3.

2.1.6   Galaxy power spectra

Most of the matter in the Universe is cold dark matter, and unfortunately we cannot measure its density distribution directly. What we can measure however is the distribution of galaxies, which form in dark matter halos. Galaxies are thus *tracers* of the underlying dark matter distribution. From the galaxy two-point correlation function, ξ_g, we can construct the galaxy power spectrum P_g and compare it to the theoretical matter power spectrum. What has been found is that galaxies are more strongly clustered than the underlying matter distribution. This leads to the concept of the so-called galaxy *bias*, i.e. galaxies are biased tracers of the underlying matter density distribution [28].

In bias models, the galaxy density δ_g is related to the matter density δ_m by some function f,

$$\delta_g = f(\delta_m). \tag{2.43}$$

The simplest bias model is the *linear bias b*,

$$\delta_g = b\delta_m. \tag{2.44}$$

Thus, the galaxy power spectrum is related to the matter power spectrum as

$$P_g = b^2 P_m. \tag{2.45}$$

A simple understanding of the bias is given within the *peak-background split* [21]. Suppose that the density contrast δ can be separated into a long-wavelength mode δ_l and a short-wavelength mode δ_s,

$$\delta = \delta_l + \delta_s. \tag{2.46}$$

Dark matter halos, and subsequently galaxies, form at regions where the total density contrast passes a certain threshold. The peaks in δ_s pass that threshold first in the large-scale crests of δ_l, not in the troughs. This leads to a stronger clustering of galaxies (see Fig. 2.4).

With the introduction of a bias factor b, it is possible to fit galaxy power spectra to the matter power spectrum (see Fig. 2.5). It turns out that galaxies at higher redshift are more strongly biased, as the first galaxies form only in the *most* overdense regions of space. It can be shown that with time the bias goes towards unity, i.e. all galaxies become unbiased tracers of the underlying matter density field [29]. For a more detailed discussion of the bias, see e.g. [22].

2.2   Relativistic cosmological perturbation theory

In the previous section we have discussed the evolution of cosmological perturbations within the Newtonian theory of gravity. We know however that Newtonian theory is wrong in that it assumes infinite speed of light and thus instantaneous gravitational interaction. From this alone it is clear that the Newtonian description of gravity is inaccurate on scales that are comparable to the horizon and larger. At these scales we need a general relativistic description of the perturbations.
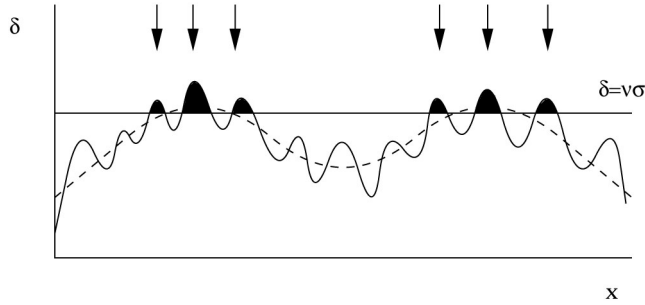
Figure 2.4: Illustration of galaxy bias. The density contrast can be separated into a long-wavelength mode (dashed) and a short-wavelength mode (solid). Galaxies form at regions where the density contrast passes a certain threshold, as indicated by the arrows. Figure from [26].
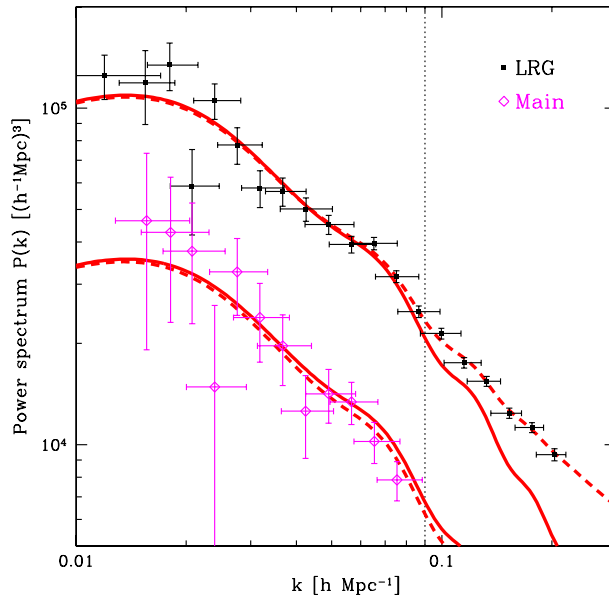
Figure 2.5: Measured galaxy power spectra for SDSS luminous red galaxies (black) and main galaxies (magenta). The solid red lines correspond to the linear matter power spectra at $z = 0$ with bias $b = 1.9$ (top) and $b = 1.1$ (bottom). The dashed red lines indicate the nonlinear correction to the power spectrum. Figure from [27].

In this subsection we will introduce relativistic cosmological perturbation theory (see also e.g. [18, 20, 30]). Our conventions are the following: Greek indices will range from 0 to 3, and Latin indices from 1 to 3, referring only to the spatial part. We will write the covariant derivative with respect to the perturbed metric as and index ';μ', and a derivative with respect to the spatial (background) coordinate x_i as ∇_i or as an index ',i'. As before, we consider perturbations in the Einstein-de Sitter model, i.e. $\Omega = \Omega_m = 1$.

2.2.1   Metric perturbations

In relativistic cosmological perturbation theory we consider perturbations in the homogenous and isotropic FRW metric tensor,

$$g_{\mu\nu} = \bar{g}_{\mu\nu} + \delta g_{\mu\nu}. \tag{2.47}$$

In a flat universe, the FRW line element can be written as

$$ds^2 = -dt^2 + a^2 d\mathbf{x}^2 = a^2(-d\tau^2 + d\mathbf{x}^2). \tag{2.48}$$

Thus, the metric tensor is diagonal,

$$\bar{g}_{\mu\nu} = a^2 \begin{pmatrix} -1 & 0 \\ 0 & \delta_{ij} \end{pmatrix}. \tag{2.49}$$

The metric perturbation can be parametrized as

$$\delta g_{\mu\nu} = a^2 \begin{pmatrix} -2\phi & w_i \\ w_i & -2e\delta_{ij} + 2h_{ij} \end{pmatrix}. \tag{2.50}$$

The metric perturbation can be further decomposed into scalar, vector and tensor parts in the following way. w_i can be decomposed as

$$w_i = w_{,i} + w_i^\perp, \tag{2.51}$$

where w is a scalar and $w_i^\perp$ is a vector, i.e. $\nabla^i w_i^\perp = 0$. h_{ij} can be decomposed as

$$h_{ij} = D_{ij}h + h_{(i,j)} + h_{ij}^{\mathrm{TT}}, \tag{2.52}$$

where $D_{ij} = \nabla_i \nabla_j - (1/3)\delta_{ij}\nabla^2$ is the symmetric traceless double-gradient operator. Here, h is a scalar, h_i is a vector (i.e. $\nabla^i h_i = 0$) and h_{ij}^{TT} is a transverse ($\nabla^i h_{ij}^{\mathrm{TT}} = 0$) and traceless ($h_i^{\mathrm{TT}\,i} = 0$) tensor.

In first order, we can neglect the couplings of perturbations. Therefore, scalar, vector and tensor perturbations can be treated independently. Here we will only focus on the perturbations that are relevant for the formation of structure, i.e. scalar perturbations. For a discussion of vector perturbations, see e.g. [18]. Tensor perturbations in the metric give rise to gravitational waves [6].

In terms of only scalar perturbations, the metric perturbation can be written as

$$\delta g_{\mu\nu} = a^2 \begin{pmatrix} -2\phi & w_{,i} \\ w_{,i} & -2\psi\delta_{ij} + 2h_{,ij} \end{pmatrix}, \tag{2.53}$$

where we have introduced the new variable

$$\psi \equiv e + \frac{1}{3}\nabla^2 h. \tag{2.54}$$

We thus have 4 degrees of freedom in the metric perturbation, corresponding to the fields ϕ, ψ, w and h.

2.2.2 Gauges and gauge transformations
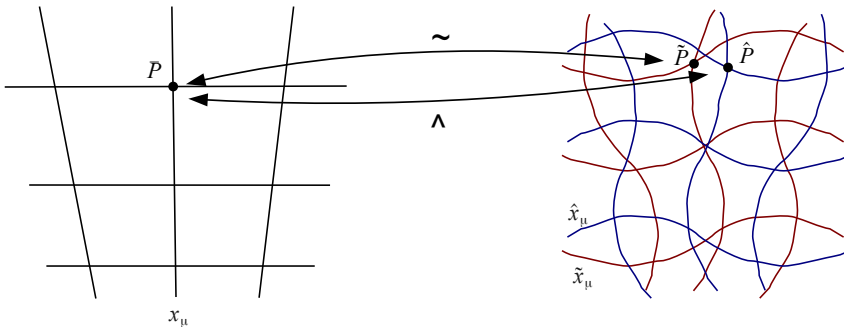
Figure 2.6: Illustration of two different gauges. The gauge '$\sim$' maps the point $\bar{P}$ in the background to the point $\tilde{P}$ in the perturbed spacetime, while the gauge '$\wedge$' maps it to the point $\hat{P}$.

One subtlety in cosmological perturbation theory arises because the splitting of the metric tensor into background and (linear) perturbations is not unique. In fact, there are infinitely many ways to perturb the spacetime metric, resulting in infinitely many 'versions' of the perturbed spacetime, which are all close to each other. This leads to the concept of *gauges* in cosmological perturbation theory. Consider a point $\bar{P}$ with coordinates x_μ in the background spacetime. Next, consider two different versions of the perturbed spacetime, with coordinates $\hat{x}_\mu$ and $\tilde{x}_\mu$. Each of these slightly different coordinate choices are what we call a *gauge*. Denote the point corresponding to $\bar{P}$ in the $\tilde{x}_\mu$-coordinates by $\tilde{P}$, and the corresponding point in the $\hat{x}_\mu$-coordinates by $\hat{P}$ (see Fig. 2.6). Then, by construction we have

$$x_\mu(P) = \hat{x}_\mu(\hat{P}) = \tilde{x}_\mu(\tilde{P}), \tag{2.55}$$

i.e. the point $\tilde{P}$ has the same coordinates in the $\tilde{x}$-coordinates as the point $\hat{P}$ in the $\hat{x}$-coordinates. The point $\hat{P}$ however has different coordinates in the $\tilde{x}$-coordinates than in the $\hat{x}$-coordinates, and we denote this small difference with the parameter ξ_μ:

$$\tilde{x}_\mu(\hat{P}) = \hat{x}_\mu(\hat{P}) + \xi_\mu, \tag{2.56}$$

This is the basic principle of a *gauge transformation*, i.e. the transformation of the spacetime-coordinates of a given point from one gauge into another gauge.

The gauge field ξ_μ can be decomposed as

$$\xi_\mu = \begin{pmatrix} \xi_0 \\ \xi_{,i} + \xi_i^\perp \end{pmatrix}, \tag{2.57}$$

where ξ_0 and ξ are scalar fields, and $\xi_i^\perp$ is a vector field with $\nabla^i \xi_i^\perp = 0$. In our analysis we only consider scalar perturbations. Thus, the field ξ_μ simplifies to

$$\xi_\mu = \begin{pmatrix} \xi_0 \\ \xi_{,i} \end{pmatrix}. \tag{2.58}$$

There are thus two gauge degrees of freedom, ξ_0, which describes the transformation in the time coordinate, and ξ, which describes the transformation in the spatial coordinates. These two degrees of freedom are unphysical and need to be fixed in any analysis of cosmological perturbations. The particular choice of the fields ξ_0 and ξ is equivalent to the choice of the gauge.

Under a gauge transformation, the perturbation of a scalar transforms as

$$\tilde{\delta s} = \hat{\delta s} - \bar{s}' \xi^0, \tag{2.59}$$

where $\bar{s}$ is the background (unperturbed) value of the scalar [31]. This means that a scalar is gauge-invariant if and only if it is constant in the background ($\bar{s}' = 0$). In particular, it follows that the density contrast transforms as

$$\tilde{\delta} = \frac{\tilde{\delta\rho}}{\bar{\rho}} = \frac{\hat{\delta\rho} - \bar{\rho}' \xi^0}{\bar{\rho}} = \hat{\delta} + 3\mathcal{H}\xi^0. \tag{2.60}$$

The peculiar velocity v^i transforms as

$$\tilde{v}^i = \frac{\mathrm{d}\tilde{x}^i}{\mathrm{d}\tilde{\tau}} = \frac{\mathrm{d}(\hat{x}^i + \xi^i)}{\mathrm{d}(\hat{\tau} + \xi^0)} \simeq \hat{v}^i + \xi^{i\prime}. \tag{2.61}$$

Finally, the metric tensor transforms as [31]

$$\tilde{g}_{\mu\nu} = \hat{g}_{\mu\nu} - \bar{g}'_{\mu\nu} - \xi_{\mu,\nu} - \xi_{\nu,\mu}. \tag{2.62}$$

From this we find the gauge transformation of the scalar fields in the metric,

$$\tilde{\phi} = \hat{\phi} - \mathcal{H}\xi^0 - \xi^{0\prime}, \tag{2.63}$$

$$\tilde{\psi} = \hat{\psi} + \mathcal{H}\xi^0, \tag{2.64}$$

$$\tilde{w} = \hat{w} + \xi^0 - \xi', \tag{2.65}$$

$$\tilde{h} = \hat{h} - \xi. \tag{2.66}$$

It is possible to define combinations of the perturbation fields that are gauge-invariant. The most commonly used gauge-invariant variables are the *Bardeen potentials* [32],

$$\Phi \equiv \phi + \frac{1}{a}[(w - h')a]', \tag{2.67}$$

$$\Psi \equiv \psi - \mathcal{H}(w - h'). \tag{2.68}$$

Another important gauge-invariant quantity is the *curvature perturbation*,

$$\zeta \equiv \frac{1}{3}\delta - \psi. \tag{2.69}$$

2.2.3   The conformal Newtonian gauge

As a particular example consider the *conformal Newtonian* gauge, or *longitudinal gauge*, which we will denote by subscript L. It is defined through the gauge condition

$$w_{\rm L} = h_{\rm L} = 0. \tag{2.70}$$

It follows that the metric potentials ϕ and ψ are equivalent to the gauge-invariant Bardeen potentials, $\phi_{\rm L} = \Phi$ and $\psi_{\rm L} = \Psi$. The line element in this gauge takes the simple form

$$ds^2 = (-1 + 2\Phi)d\tau^2 + (1 - 2\Psi)\delta_{ij}dx^i dx^j. \tag{2.71}$$

The energy-momentum tensor for a perfect fluid with zero pressure is generally given by

$$T^\mu_\nu \equiv \rho u^\mu u_\nu = \bar{\rho}(1+\delta)u^\mu u_\nu. \tag{2.72}$$

From the normalization of the 4-velocity, $g_{\mu\nu}u^\mu u^\nu = -1$, it follows that

$$u^\mu = \frac{1}{a}\left(\begin{array}{c} 1 - \Phi \\ v_{{\rm L},i} \end{array}\right) \;,\; u_\mu = a\left(\begin{array}{c} -1 - \Phi \\ v_{{\rm L},i} \end{array}\right), \tag{2.73}$$

where we introduced the peculiar velocity potential $v_{\rm L}$. The peculiar velocity can be written as a gradient of that potential, $\mathbf{v}_{\rm L} = \nabla v_{\rm L}$, because here we only consider scalar perturbations. Thus, the energy-momentum tensor can be written as

$$T^\mu_\nu = \bar{\rho}\left(\begin{array}{cc} -(1+\delta_{\rm L}) & v_{{\rm L},i} \\ -v_{{\rm L},i} & 0 \end{array}\right). \tag{2.74}$$

Evolution equations for the perturbed fields can then be found from the energy-momentum conservation equation,

$$T^\mu_{\nu;\mu} = 0. \tag{2.75}$$

At the background level, this gives the continuity equation,

$$\bar{\rho}' + 3\mathcal{H}\bar{\rho} = 0. \tag{2.76}$$

At linear order we find two equations, corresponding to the $(0,0)$-component and the $(0,i)$-components,

$$\delta'_{\rm L} + \nabla^2 v_{\rm L} - 3\Psi' = 0, \tag{2.77}$$
$$\nabla v'_{\rm L} + \mathcal{H}\nabla v_{\rm L} = -\nabla\Phi. \tag{2.78}$$

These equations are remarkably similar to the continuity equation and the Euler equation in the Newtonian analysis discussed earlier. This is the reason why the Bardeen potential Φ in relativistic theory can be identified with the Newtonian gravitational potential. Note however that in the relativistic version of the continuity equation there appears an additional term $-3\Psi'$. Thus, only for constant Ψ we find an exact agreement with the Newtonian equations.

What is missing now is the relativistic counterpart to the Poisson equation. For this, consider the Einstein equation,

$$G^{\mu}_{\nu} = 8\pi G T^{\mu}_{\nu}. \tag{2.79}$$

The perturbed Einstein tensor can be derived from the metric (see Appendix) and is given by:

$$
\begin{aligned}
G^0_0 &= -3a^{-2}\mathcal{H}^2 + a^{-2}[2\nabla^2\Psi + 6\mathcal{H}\Psi' + 6\mathcal{H}^2\Phi], \\
G^0_i &= -2a^{-2}(\Psi' + \mathcal{H}\Phi)_{,i}, \\
G^i_0 &= 2a^{-2}(\Psi' + \mathcal{H}\Phi)_{,i}, \\
G^i_j &= a^{-2}(-2\mathcal{H}' - \mathcal{H}^2)\delta^i_j \\
&\quad + a^{-2}[2\Psi'' + \nabla^2(\Phi - \Psi) + \mathcal{H}(2\Phi' + 4\Psi') + (4\mathcal{H}' + 2\mathcal{H}^2)\Phi]\delta^i_j \\
&\quad + a^{-2}(\Psi - \Phi)_{,ij}.
\end{aligned}
$$

In the background order, the (0,0)-component and the trace of the (i,j)-components of the Einstein equation give the Friedmann equations,

$$\mathcal{H}^2 = \frac{8\pi G}{3}\bar{\rho}a^2, \tag{2.80}$$

$$\mathcal{H}' = -\frac{4\pi G}{3}\bar{\rho}a^2. \tag{2.81}$$

In first order, we have in total four equations, corresponding to the (0,0)-component, the (0,i)-components, and the trace and traceless part of the (i,j)-components of the Einstein equation:

$$3\mathcal{H}^2\Phi + 3\mathcal{H}\Psi' - \nabla^2\Psi = -\frac{3}{2}\mathcal{H}^2\delta_{\mathrm{L}}, \tag{2.82}$$

$$\Psi' + \mathcal{H}\Phi = -\frac{3}{2}\mathcal{H}^2 v_{\mathrm{L}}, \tag{2.83}$$

$$
\begin{aligned}
3\Psi'' + 3\mathcal{H}(\Phi' + 2\Psi') + \nabla^2(\Psi - \Phi) & \\
+(2\mathcal{H}' + \mathcal{H}^2)\Phi &= 0, \tag{2.84}
\end{aligned}
$$

$$(\Psi - \Phi)_{,ij} = 0. \tag{2.85}$$

The (0,0)-component is the relativistic counterpart of the Poisson equation. The other equations however do not have any relation to Newtonian theory.

The solutions to the evolution equations can be easily expressed in momentum space,

$$\Phi = \Psi = \mathrm{const}, \tag{2.86}$$

$$\delta_{\mathrm{L}} = -2\Phi - \frac{2}{3}\frac{k^2}{\mathcal{H}^2}\Phi, \tag{2.87}$$

$$v_{\mathrm{L}} = -\frac{2}{3}\frac{\Phi}{\mathcal{H}}. \tag{2.88}$$

Thus, if we identify the metric potential Φ with the Newtonian gravitational potential, then the velocity field in this gauge is identical with the velocity field in
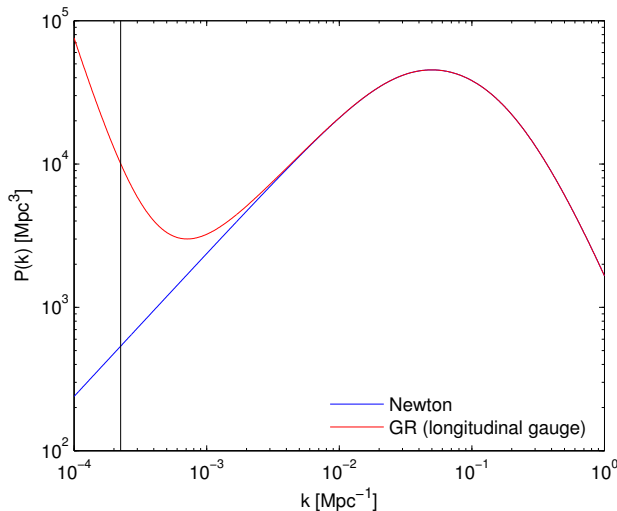
Figure 2.7: Linear matter power spectrum today, according to Newtonian theory (blue) and relativistic cosmological perturbation theory in longitudinal gauge (red). The black line corresponds to the comoving horizon today. Newtonian and relativistic theory are in good agreement for scales much smaller than the horizon.

Newtonian theory. The density contrast in this gauge agrees with its Newtonian counterpart on sub-horizon scales $k/\mathcal{H} \gg 1$. On super-horizon scales however $(k/\mathcal{H} \ll 1)$, the density contrast is constant, $\delta_{\mathrm{L}} = -2\Phi$. On these scales, the relativistic matter power spectrum differs thus from the Newtonian one, see Fig. 2.7. The agreement between Newtonian and relativistic theory on sub-horizon scales can be related to the fact that the misconception of Newtonian gravity, instantaneous gravitational interaction, is less severe on these small distance scales.

The results here were derived in the longitudinal gauge. There exist however many other gauges, in which the relativistic-Newtonian correspondence changes. A comparison between several different gauges is presented in Ref. [1]. For instance, in the *synchronous gauge*, which in the case of an Einstein-de Sitter model corresponds to the *comoving gauge*, the relativistic density contrast is identical with the Newtonian one on all scales. However, in that gauge there are no peculiar velocities. It is also possible to construct a gauge in which both the density contrast and the peculiar velocities agree with their corresponding Newtonian quantities at all scales. This is possible because in relativistic cosmological perturbation theory we have two gauge degrees of freedom. Such a gauge is introduced as the *Newtonian matter gauge* in Ref. [1], and some interesting implications are derived. For instance, in this gauge there are perturbations in the Hubble rate present, which do not exist in the Newtonian description. Thus, even though the relativistic-Newtonian correspondence is given at the level of matter densities and velocities, the Hubble rate is different.

Because the relativistic-Newtonian correspondence is not necessarily given at large scales, care must be taken in the interpretation of cosmological N-body simulations, which are based on Newtonian equations of motion. Relativistic corrections can however be incorporated into the simulations by solving additional equations [33, 34]. Efforts towards cosmological N-body simulations based on general relativistic theory are currently being made [35].

Finally we note that quantities which are based on observations, such as galaxy correlation functions or galaxy power spectra, should of course be gauge-independent. In order to compare theory to observations, it is thus important to derive gauge-invariant expressions for these observable quantities. For instance, one needs to take into account the fact that we only observe galaxies on our past lightcone. Furthermore, we do not measure true spatial positions, but positions in redshift space, where the peculiar velocities of galaxies change the observed redshift, leading to the so-called *redshift space distortions*. For a more detailed discussion of these observational aspects, see e.g. [36, 37, 38, 39].

Chapter 3

Dark Energy and the integrated Sachs-Wolfe effect

3.1 Dark Energy - models and observations

When Albert Einstein developed his theory of General Relativity in 1917, it was not yet discovered that the Universe is expanding. In order to construct a static solution to the Friedmann equation, he introduced a constant Λ into his field equation, which would counteract the pull of gravity. At the same time, Willem de Sitter showed that in a universe consisting only of a cosmological constant, space would be expanding, and in fact with an accelerating rate. We refer to his model today as the *de Sitter* model. After Hubble's observation in 1929 that space *is* expanding, Einstein realized that the constant term in his equation was a mistake. Without it, his field equation would describe correctly the expanding Universe. Today, observations indicate that the Universe is in fact in a state of accelerated expansion. Einstein's constant Λ re-appeared in the equation in order to explain this accelerated expansion, like in de Sitter's model.

Historically, the first indications towards a cosmological constant appeared around 1990, when studies of large-scale galaxy clustering implied a low energy density of matter, $\Omega_{\mathrm{m}} = 0.15 - 0.4$ [40, 41]. This is however in contrast to inflationary theories, which predict a spatially flat Universe, i.e. $\Omega_{\mathrm{tot}} \simeq 1$. Therefore the existence of a further component with an energy density $\Omega = 1 - \Omega_{\mathrm{m}}$ would be needed. In the middle of the 1990s, there were thus two competing models, the flat ΛCDM model on the on hand, and the open CDM model on the other hand. From both models predictions for the large-scale structure of the Universe could be derived, given the amplitude of the CMB temperature fluctuations; the predictions from ΛCDM were however in better agreement with observations [42]. Further, the age of some globular clusters seemed to be in contrast with the age of the Universe in the open CDM model [43, 44]. Therefore, the combination of data from large-scale structure, CMB anisotropies, Hubble rate, and predictions from inflation favoured the ΛCDM model.

A promising way to probe cosmic acceleration is to measure the distance to

far objects as a function of their redshift. In astronomy, the distance to an object is measured in terms of its *distance modulus* $m - M$, where m is its apparent magnitude and M is its absolute magnitude. The distance modulus is related to the *luminosity distance* d_{L} (in Mpc) as

$$m - M = 25 + 5\log_{10} d_{\mathrm{L}}. \tag{3.1}$$

It would therefore be helpful to have *standard candles*, i.e. objects with known absolute magnitude M, so that the luminosity distance for a given redshift can be determined. Supernovae of Type Ia are considered as *standardizable candles* because of the tight correlation between their peak luminosity and the shape of their light curve. The luminosity distance of these supernovae can therefore be estimated [45, 46]. In 1998, two teams independently found that supernovae at high redshift are dimmer than expected in a matter dominated universe [47, 48]. Both teams interpreted their results as evidence for cosmic acceleration caused by a nonzero cosmological constant. Shortly after the supernovae results, balloon-borne CMB experiments measured with high precision the angular position of the first acoustic peak, which implied $\Omega_{\mathrm{tot}} = 1$ [49, 50]. Given the low value of Ω_{m}, this result is a further confirmation for ΛCDM.

Today we have a broad range of different observational probes, including more supernovae data over a wider redshift range, more precise CMB data, measurements of the baryon acoustic oscillation scale in galaxy clustering, weak gravitational lensing measurements of dark matter clustering, and more precise measurements of H_0, which all favour the ΛCDM model (see Fig. 3.1). For a detailed review, see [8].

Attempts were made to explain the cosmological constant within theoretical particle physics. It is known that the vacuum energy of a quantum field is usually nonzero (for a review of quantum field theory, see e.g. [51]). It would thus be a natural solution if the cosmological constant were simply the vacuum energy predicted in quantum field theories. However, it turns out that the natural vacuum energy is much larger, by about 120 orders of magnitude, than the measured value for the cosmological constant. This is the *cosmological constant problem*.

There are several alternative explanations to the cosmological constant Λ for the accelerated expansion. From the Raychaudhuri equation we have

$$\frac{\ddot{a}}{a} = -\frac{4\pi G}{3}\rho(1 + 3w). \tag{3.2}$$

Thus, any energy component with $w < -1/3$ causes the expansion to accelerate ($\ddot{a} > 0$). Generally, we call such an energy component *dark energy*. Dark energy can for example have the form of a light scalar field, characterized by the shape of its potential. These are the so-called *quintessence*-models. Models with $w < -1$ are the so-called *phantom* models. In phantom models, the dark energy density *increases* with time, making the expansion of space so fast that ultimately all structure is destroyed in the so-called *Big Rip* [52]. The accelerated expansion can alternatively be explained within modified gravity models. Yet another approach is to relax the assumption of homogeneity and explain the apparent accelerated expansion with an inhomogeneous metric. For a more detailed overview over dark
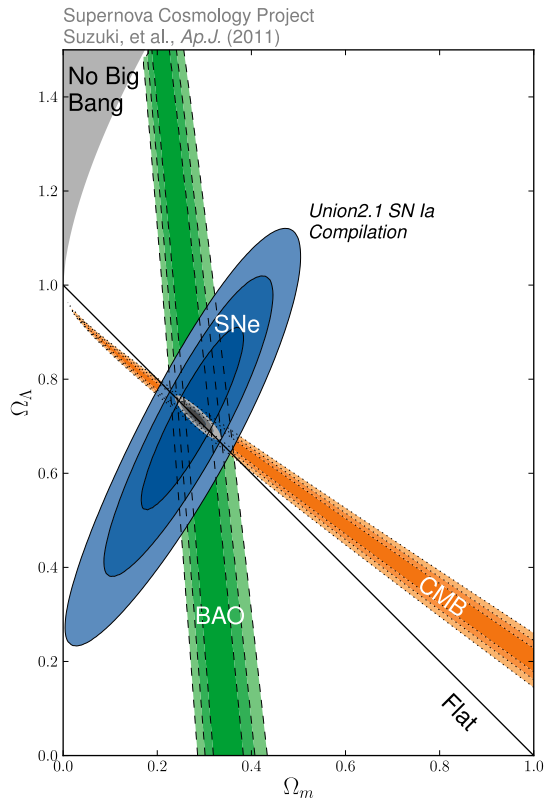
Figure 3.1: Constraints on Ω_Λ and Ω_m. The figure shows the 68%, 95%, and 99.7% C.L. constraints on Ω_Λ and Ω_m obtained from CMB data (orange), BAO data (green), and supernovae data (blue). The grey contours show the combined constraints. All datasets are consistent with a flat universe with $\Omega_m \simeq 0.3$ and $\Omega_\Lambda \simeq 0.7$. Image credit: Supernova Cosmology Project.

energy models, see e.g. [53, 54]. In the following, we will focus only on dark energy in form of a cosmological constant Λ.

3.2 FRW universe with Λ - background and perturbations

In a universe consisting of cold dark matter, described by the energy-momentum tensor $T_{\mu\nu}$, and dark energy in form of a cosmological constant Λ, the Einstein equation can be written as

$$G_{\mu\nu} + \Lambda g_{\mu\nu} = 8\pi G T_{\mu\nu}. \tag{3.3}$$

Alternatively, the cosmological constant could also be written on the right hand side of the Einstein equation, as part of the energy-momentum tensor. There is thus an ambiguity whether the cosmological constant is part of the geometry of the universe, or part of its content. In any case, the Friedmann equations then take the form

$$H^2 = \frac{8\pi G}{3}\bar{\rho}_{\mathrm{m}} + \frac{\Lambda}{3}, \tag{3.4}$$

$$\frac{\ddot{a}}{a} = \frac{\Lambda}{3} - \frac{4\pi G}{3}\bar{\rho}_{\mathrm{m}}. \tag{3.5}$$

From the second Friedmann equation we see that a nonzero cosmological constant allows $\ddot{a} > 0$, i.e. accelerated expansion.

A particular solution can be expressed in terms of hyperbolic functions [55],

$$a(t) = \left(\frac{\Omega_{\mathrm{m}}}{1 - \Omega_{\mathrm{m}}}\right)^{1/3} \sinh^{2/3}\left(\frac{t}{t_{\Lambda}}\right), \tag{3.6}$$

$$H(t) = \frac{2}{3t_{\Lambda}}\coth\left(\frac{t}{t_{\Lambda}}\right), \tag{3.7}$$

$$\bar{\rho}_{\mathrm{m}}(t) = \frac{\Lambda}{8\pi G}\sinh^{-2}\left(\frac{t}{t_{\Lambda}}\right), \tag{3.8}$$

where $t_{\Lambda} = 2/\sqrt{3\Lambda}$.

Let us now consider matter perturbations in a universe which contains a cosmological constant. If we neglect dark energy perturbations, then the only change compared to the Einstein-de Sitter model discussed earlier is at the background level, while the perturbation equations remain the same. In particular, the growth of the density contrast is still given by the Jeans equation,

$$\delta'' + \mathcal{H}\delta' = 4\pi G\bar{\rho}_m a^2 \delta. \tag{3.9}$$

During dark energy domination, the source term in this differential equation is decaying exponentially, and the dominating solution becomes

$$\delta \sim \mathrm{const}, \tag{3.10}$$
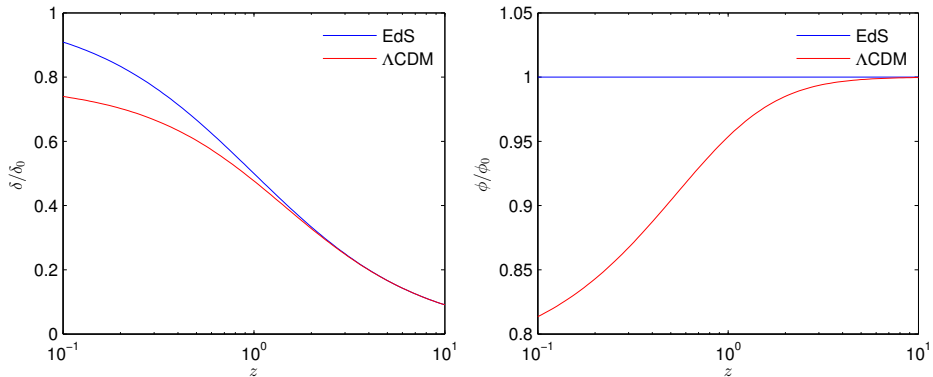
Figure 3.2: Evolution of the density contrast (left) and the gravitational potential (right) as a function of redshift, in the Einstein-de Sitter model ($\Omega_\Lambda = 0$, $\Omega_m = 1$) (blue), and ΛCDM ($\Omega_\Lambda = 0.7$, $\Omega_m = 0.3$) (red). The decay of the gravitational potential in ΛCDM after $z \sim 10$ causes the ISW effect.

i.e. the density contrast freezes out. In order to find the time-evolution of the gravitational potential, consider the Poisson equation,

$$\nabla^2 \phi = 4\pi G a^2 \bar{\rho}_m \delta \sim \frac{\delta}{a}. \tag{3.11}$$

From this it can be seen that perturbations in the gravitational potential decay as $\phi \sim a^{-1}$ (see Fig. 3.2).

3.3 The integrated Sachs-Wolfe effect

3.3.1 Theory of the ISW effect

The decay of the gravitational potential affects the temperature of CMB photons in the following way. Consider an overdense region, i.e. a potential well, in the local large-scale structure. When a CMB photon falls into the potential well, it gains some energy ΔE_1. By the time the photon leaves the overdense region, the potential well has become a bit shallower due to its decay, and the photon loses some energy $\Delta E_2 < \Delta E_1$. Thus, the photon gains some net energy $\Delta E_1 - \Delta E_2 > 0$. CMB photons passing an overdense region in the local large-scale structure will thus appear slightly hotter. In the same way, CMB photons passing an underdense region will appear colder. This effect is called the (late) *integrated Sachs-Wolfe* (ISW) effect [17]. As discussed previously, there exists also an early ISW effect, due to the decay of the gravitational potential for a short period of time after last scattering, while the Universe was not yet completely matter dominated. However, here we are only interested in the late ISW effect, as it can be used to probe the dynamical effects of dark energy.

The integrated Sachs-Wolfe temperature signal in direction $\mathbf{n}$ is given by

$$\Delta T_{\mathrm{ISW}}(\mathbf{n}) = 2\bar{T}_0 \int_0^{r_{\mathrm{LS}}} \dot{\phi}(r, z, \mathbf{n}) a \, dr, \qquad (3.12)$$

where $\bar{T}_0$ is the mean temperature of the CMB, and $r_{\mathrm{LS}} \simeq 14\,\mathrm{Gpc}$ is the distance to the last scattering surface. The gravitational potential ϕ is related to the density contrast via the Poisson equation,

$$\nabla^2 \phi(\mathbf{x}, t) = 4\pi G \bar{\rho}_{\mathrm{m}}(t) a^2 \delta(\mathbf{x}, t). \qquad (3.13)$$

Changing to Fourier space and taking the time derivative gives

$$\dot{\phi}(\mathbf{k}, t) = \frac{3}{2} \left(\frac{H_0}{k}\right)^2 \Omega_{\mathrm{m}} \left[\frac{\dot{a}}{a^2} \delta(\mathbf{k}, t) - \frac{\dot{\delta}(\mathbf{k}, t)}{a}\right]. \qquad (3.14)$$

In linear approximation we have $\delta(\mathbf{k}, t) = D(t)\delta(\mathbf{k}, z = 0)$, where $D(t)$ is the linear growth factor. Substituting this into Eq. (3.14) yields:

$$\dot{\phi}(\mathbf{k}, z) = \frac{3}{2} \left(\frac{H_0}{k}\right)^2 \Omega_{\mathrm{m}} \frac{H(z)}{a} [1 - \beta(z)] \delta(\mathbf{k}, z), \qquad (3.15)$$

where $\beta(t) \equiv \mathrm{d}\ln D / \mathrm{d}\ln a$ denotes the linear growth rate. Note that during matter domination we have $D \sim a$, so that $\beta = 1$ and thus $\dot{\phi} = 0$, i.e. the potential is constant. If we assume spherical symmetry of the structures, Eq. (3.15) may be rewritten in real space as

$$\dot{\phi}(r, z) = \frac{3}{2} \Omega_{\mathrm{m}} H_0^2 G(z) F(r), \qquad (3.16)$$

where $G(z) = H(z)(1 - \beta(z))D(z)/a$ is the ISW linear growth factor and $F(r)$ is given by

$$F(r) = \int_0^r \frac{r'^2}{r} \delta(r') \mathrm{d}r' + \int_r^\infty r' \delta(r') \mathrm{d}r', \qquad (3.17)$$

with $\delta(r')$ evaluated at $z = 0$.

The above derivation of the ISW temperature signal holds in the linear regime. As discussed earlier, nonlinear contributions need to be taken into account as the density contrast becomes close to unity. The nonlinear contribution to the density contrast causes a nonlinear contribution to the ISW signal, the so-called *Rees-Sciama* contribution [56]. In linear order, the ISW effect occurs because the growth of the density contrast slows down. The second order contributions to the density contrast grow faster than the first order contributions. Therefore, the nonlinear contribution to the ISW effect, the Rees-Sciama effect, has the opposite sign, i.e. it weakens the ISW signal.

3.3.2 Observation of the ISW effect

At the level of the CMB angular power spectrum, the ISW effect causes a tilt in the Sachs-Wolfe plateau at multipoles $\ell < 10$, as seen in Fig. 1.4. However,

500-1500 Mpc/h

-19.7μK   18.2μK
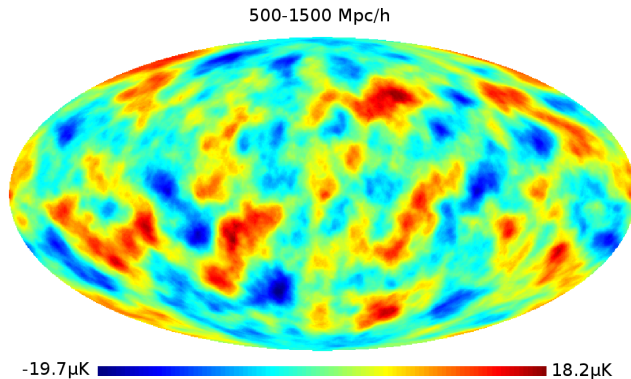
Figure 3.3: Simulated ISW temperature map. The map shows the ISW signal caused by superstructures within a comoving distance from $500 - 1500 \, h^{-1}$ Mpc. It was created by tracing photon paths through an N-body simulation and calculating the ISW temperature signal from Eq. (3.12) along each photon path. Figure taken from [57].

due to the large cosmic variance at those angular scales, a statistically significant detection of the ISW effect from the angular power spectrum alone is not possible.

At the level of the CMB map, the ISW effect causes the appearance of hot spots and cold spots in the directions of over- and underdense regions in the local large-scale structure (see Fig. 3.3). Unfortunately however, the amplitude of these secondary temperature fluctuations is about an order of magnitude smaller than the amplitude of the primordial CMB temperature fluctuations. This makes a direct detection of the ISW signal from the CMB temperature map impossible.

In [58] it was pointed out that a measurement of the ISW effect is possible by cross-correlating the CMB map with tracers of local large-scale structure, e.g. galaxies. This method is limited due to the dominating primordial CMB temperature anisotropies, but with a full-sky galaxy survey a detection with a statistical significance of up to 7.6σ is theoretically possible [59]. Several such studies have been performed in the recent years, with results ranging from 0σ to 4σ (for an overview see [60]). In [59] the data sets from several galaxy surveys were combined, yielding a detection of the ISW signal with a combined statistical significance of 4.4σ. The Planck collaboration reports a 3σ detection by cross-correlation of the CMB with SDSS and NVSS data, and a 2.5σ detection by cross-correlation with the Planck lensing map [61]. With the next generation of large galaxy surveys, like the Dark Energy Survey and Euclid, the significance of the detection of the ISW effect will certainly improve.

The problem with the cross-correlation method is not only the fact that the primordial CMB temperature fluctuations are dominating, but also the existence of *shot noise* in galaxy surveys, which makes it difficult to reconstruct the underlying matter density field. This motivated the authors of Ref. [62] to perform a different

type of analysis. Their goal was to detect the ISW signal by stacking patches of the CMB along the lines of sight of the most extreme superstructures (overdensities and underdensities) in the local large-scale structure, and applying aperture photometry to the stacked CMB image. In theory, these overdensities and underdensities are aligned with hot and cold spots, respectively, in the CMB, which therefore would lead to a detection of the ISW temperature signal from the CMB stacks. Using this method, the authors report a detection of the combined ISW temperature signal from overdensities and underdensities of $\Delta T_{\mathrm{ISW}} = (9.6 \pm 2.2)\,\mu\mathrm{K}$, i.e. a statistical significance of 4.4σ.

Unfortunately however, the authors of [62] do not give a theoretical expectation for the magnitude of the ISW temperature signal so obtained. It was first pointed out in [63] that the magnitude of this signal is in fact too large and in tension with its prediction from the ΛCDM model. This study was updated in [64], where it was shown that the tension with ΛCDM is at the $> 3\sigma$ level. The theoretical expectation for the stacked ISW signal in [64] was derived under the assumptions that all structures are spherical and all perturbations are in the linear regime. It is therefore important to know how much the ISW signal gets boosted by non-sphericity of the structures and non-linear contributions. The study in [64] is updated in Ref. [2] and complemented by the results for the stacked ISW signal from N-body simulations, in which neither of these assumptions are being made. The simulations confirm that the signal found in [62] is discrepant with its ΛCDM prediction at the $> 3\sigma$ level. In fact, because of the weakness of the ISW effect, one would not expect to detect any significant signal at all in this kind of measurement.

It is thus not clear what caused the signal found in [62]. One possibility is of course that it is just a statistical fluke. Note however that a fluke with this statistical significance is very rare (around one in $100\,000$, assuming a Gaussian distribution). On the other hand, if the signal is not just a statistical fluke, it might be an important hint towards new physics beyond the standard model. For instance, the signal could be explained in non-Gaussian models, where the most extreme structures are even more extreme and more abundant, leading to a boost of the ISW effect. It was shown in [65] that such a boost of the ISW signal does exist in models with nonzero f_{NL}, however it is very weak: for $f_{\mathrm{NL}} = \pm 100$, the authors report a boost of only $\Delta T < 0.1\,\mu\mathrm{K}$, too little to explain the signal observed in [62]. A study with nonzero g_{NL} was not performed, and remains a possibility. Alternatively, the signal might also be explained in modified gravity models or models in which dark energy has not the form of a cosmological constant. In any case, exploring the nature of this puzzling signal might give insights about physics beyond ΛCDM.

Chapter 4

The hemispherical power asymmetry

4.1 CMB anomalies and statistics

The statistical properties of the measured CMB can be remarkably well described within the ΛCDM model. From the angular power spectrum alone, no evidence is found for the existence of e.g. additional matter or radiation species, isocurvature in the primordial fluctuations, or a primordial power spectrum that is not described by a power law [4]. However, on the largest angular scales of the CMB, some features have been found that are unlikely to appear within the ΛCDM model, the so-called CMB *anomalies*. Among them are a lack of power in the low multipoles, an alignment of the quadrupole and octopole with each other and with the ecliptic plane along the so-called *axis of evil*, a hemispherical power asymmetry, a parity asymmetry in the lowest multipoles, and the so-called *Cold Spot*. Those anomalies were first found in the WMAP data [66, 67], and later confirmed, with similar statistical significances, in the new Planck data [68].

Statistical fluctuations are everywhere in the data. An important question in data analysis is thus whether a feature found in the data is a real, physical signal or just a statistical fluctuation, a fluke. The answer to this question is usually given in terms of the p-value, which gives the probability that the observed feature could have been seen by chance. In practice, the p-value cannot always be calculated directly. What is therefore often used instead is the *statistical significance* of the feature in terms of standard deviations away from the mean. A statistical significance of $z\sigma$ means that the measured value lies z standard deviations into the tail of the probability distribution of possible values. Assuming a Gaussian probability distribution function, the statistical significance can be translated into the p-value as

$$p = 1 - \mathrm{erf}\left(\frac{z}{\sqrt{2}}\right). \qquad (4.1)$$

For a conversion between the values of z and the p-value, see Tab. 4.1. In physics, a feature in the data is conventionally considered as a detection of a physical

significance	p-value
1σ	0.32
2σ	0.046
3σ	0.0027
4σ	$6.3 \cdot 10^{-5}$
5σ	$5.7 \cdot 10^{-7}$

Table 4.1: Relation between statistical significance $z\sigma$ and p-value in a Gaussian probability distribution function.

signal if its statistical significance is at least 5σ, i.e. the probability of it occurring by chance is less than one in a million (assuming a Gaussian distribution). For instance, the announcement of the discovery of the Higgs-boson in 2012 was based on a 5σ-detection.

The amount of data encoded in the CMB temperature anisotropies is immensely large. For instance, the CMB temperature maps from Planck have a resolution of around 50 million pixels. There is a huge number of possible statistical tests that could be applied to that data. It is thus expected that, after many different statistical tests have been applied, under some of them the data will show some statistically significant features, even though our understanding of the underlying physics is correct. This is the so-called *look-elsewhere effect*. For example, a feature with a p-value of 0.05, i.e. a statistical significance of $\sim 2\sigma$, is likely to occur after 20 different statistical tests have been applied. This is particularly dangerous if we first see the data and then choose a statistical test that is sensitive to a particular feature seen in the data. This is what we refer to as *a posteriori* statistics. Ideally, statistical tests in physics should be chosen *a priori*, i.e. prior to seeing the data, based on theoretical considerations alone.

In particle physics, the problem of the look-elsewhere effect can be alleviated by building different detectors. If a statistically significant feature is observed in one detector, but not in the other, it is likely to be a statistical fluke. If it however shows up in both detectors, it is probably a detection. The discovery of the Higgs-boson was based on a 5σ-detection in both the CMS [69] and ATLAS [70] detector, which removes the possibility of a look-elsewhere effect. In cosmology however, the situation is more bleak. We only have one CMB sky, i.e. any statistical test can only be applied once. There is no easy way of removing the look-elsewhere effect like in particle physics.

The anomalies found in the CMB data are features with statistical significances of $\sim 3\sigma$. However, because of the unquantified look-elsewhere effects and possible *a posteriori*-statistics in their detection, their interpretation is not clear. They might point towards new physics, or might just be statistical flukes.

An alternative approach in data analysis is *Bayesian statistics*. In contrast to *frequentist statistics*, where the only quantity of interest is the p-value, Bayesian statistics is a tool to compare different theoretical models. Given a model M with

parameters θ, one is primarily interested in the *Bayesian evidence* for the model in light of the data d,

$$E = P(d|M) = \int \mathrm{d}\theta P(d|\theta, M) P(\theta|M), \tag{4.2}$$

which is simply the average likelihood $P(d|\theta, M)$ over the model *prior* $P(\theta|M)$. Given two models, e.g. a simple model and a more complicated model with additional parameter, one can then calculate the evidence log ratio $\Delta \ln E$. The support for the more complicated model can be categorized as either 'inconclusive' ($\Delta \ln E < 1$), 'weak' ($1 \leq \Delta \ln E < 2.5$), 'moderate' ($2.5 \leq \Delta \ln E < 5$), or 'strong' ($\Delta \ln E \geq 5$) - this is the so-called *Jeffrey's scale* [71]. For comparison, $\Delta \ln E = 5$ corresponds to betting odds of 150:1 in favour of the more complicated model.

The advantage of Bayesian statistics is that it provides a framework in which a decision for or against a particular model can be made. However, such a model must exist in the first place, which is for instance not the case for all of the CMB anomalies. Another problem is that it not always clear how to choose the prior for a model. The choice of the prior is particularly important in model comparison because it influences the obtained evidence ratios.

Put in simple terms, the question asked in the two statistical approaches is a different one. While frequentists ask 'How likely is the data given the model?', Bayesians ask 'How likely is the model given the data?'. If several models exists, then the Bayesian approach can tell which one is the best in light of the data. If only one model exists, then the Bayesian approach is not available. In that case, the frequentist approach can tell where the model is in tension with the data. This tension can motivate the construction of new models, which can then be compared to the original one with a Bayesian analysis. In that sense, Bayesian and frequentist methods do not have to be regarded as competitive, but rather as complementary. The use of Bayesian tools in cosmology has increased in the recent years - for a detailed review, see [72].

4.2 The hemispherical power asymmetry - observation and theories

In their analysis of the first-year WMAP CMB data, Eriksen et al [74] and Hansen et al [75] found that the angular power of the CMB appears to be anisotropic (see Fig. 4.1). In particular, it was shown that the hemisphere centred at Galactic coordinates $(l, b) = (237°, -20°)$ has significantly more power than the opposite one, in the multipole range $\ell = 2 - 40$. The authors report a *p*-value of ~ 0.01.

As pointed out in [67], one problem with this initial study is the *a posteriori* choice of the maximum multipole range considered. It is therefore important to investigate whether the asymmetry found in the low multipoles persists also in higher multipoles. If it does, then this can be considered as further evidence for a physical cause of the asymmetry, as all multipoles are in principle independent of each other. Such a study was performed in a follow-up analysis by Hansen
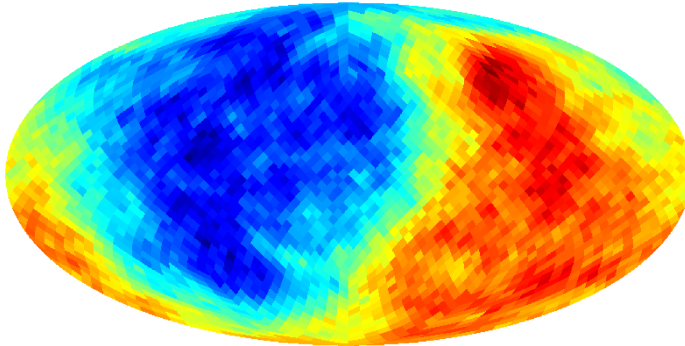
Figure 4.1: The hemispherical power asymmetry. Each pixel in the map shows the average power in the multipoles $\ell = 2 - 101$, calculated in the hemisphere centred at that pixel. The color scale ranges from $0.037\,\mu\mathrm{K}^2$ (blue) to $0.041\,\mu\mathrm{K}^2$ (red). The asymmetric shape is evident. Figure from [73].

et al [73], and it was shown that the asymmetry persists, in a similar direction, in the whole multipole range $\ell = 2 - 600$. With the new Planck CMB data, it is possible to study the hemispherical asymmetry at even higher multipoles. A detailed analysis of the multipoles $\ell = 601 - 2048$ is presented in Ref. [3]. The main result is that the asymmetry disappears at these multipoles.

In [76] it was shown that the hemispherical power asymmetry can be described in terms of a *dipolar modulation* in the CMB temperature anisotropies. This is a modulation of the form

$$\delta T = \delta T_{\mathrm{iso}}(1 + A\mathbf{p} \cdot \mathbf{n}), \tag{4.3}$$

where $\mathbf{n}$ is the direction of observation, $\mathbf{p}$ is the direction of the asymmetry axis, and A is the amplitude of the modulation. Using this parametrization, it is possible to perform a Bayesian model comparison: ΛCDM versus ΛCDM including a dipolar modulation with additional parameter A. This was done by Eriksen et al [77], who report a log evidence ratio of $\Delta \ln E = 1.8$ ('weak') for a dipolar modulation in the multipoles $\ell \leq 40$. Hoftluft et al [78] consider a larger multipole range, $\ell \leq 64$, increasing the evidence for the more complicated model to $\Delta \ln E = 2.6$ ('moderate'). It is however important to note that these log evidence ratios depend also on the prior for the more complicated model, which is chosen to be $A \leq 0.3$ by Eriksen et al, and $A \leq 0.15$ by Hoftluft et al. Weaker support for the more complicated model would have been found with a larger prior volume, as was pointed out in [79].

After the discovery of the hemispherical power asymmetry, several theoretical models have been proposed in which the creation of this anomaly is explained within the context of inflation, see e.g. [80, 81, 82, 83]. For example, a dipolar modulation can be created by a large-amplitude super-horizon perturbation in the field that generates the primordial curvature perturbations [80] (see Fig. 4.2). It was found that such a scenario is not possible in standard slow-roll inflation
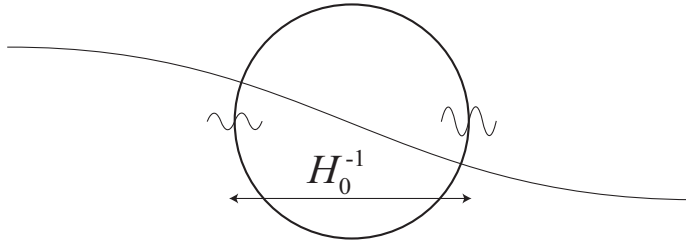
Figure 4.2: Illustration of a super-horizon perturbation, i.e. a perturbation on a scale $k^{-1} \gg H_0^{-1}$. In curvaton models, such a perturbation can cause a dipolar modulation in the primordial curvature perturbation field. Figure from [80].

without violating constraints on the homogeneity of the Universe. It is however possible in the *curvaton* model [84, 85, 86]. This is a two-field model of inflation, in which the inflaton causes exponential expansion of space, while another field, the *curvaton*, generates perturbations in the curvature. The authors of [80] also show that this model for the creation of the hemispherical asymmetry makes certain predictions for the CMB polarization, which might be testable with future experiments.

The analysis in [80] was repeated in [83] with current data and fewer constraints on the shape of the curvaton potential. The author derives a consistency relation between the dipolar modulation amplitude A and the non-Gaussian parameter f_{NL} in the curvaton-scenario,

$$|A(k)| \lesssim 0.018|f_{NL}(k)|^{1/2}. \tag{4.4}$$

From the existence of the hemispherical asymmetry at low multipoles we know that [68]

$$A(k) = 0.07 \pm 0.02 \text{ at } k^{-1} \sim 1\,\text{Gpc}. \tag{4.5}$$

A small-scale constraint on $A(k)$ comes from the distribution of high-redshift quasars found in the SDSS [87],

$$|A(k)| < 0.012 \text{ at } k^{-1} \sim 1\,\text{Mpc}, \tag{4.6}$$

at 95% C.L. In Ref. [3], the absence of an asymmetry in the multipoles $\ell = 601 - 2048$ is translated into an even tighter constraint on the modulation amplitude, which is derived under extremely conservative assumptions,

$$|A(k)| < 0.0045 \text{ at } k^{-1} \sim 10\,\text{Mpc}, \tag{4.7}$$

at 95% C.L. We can thus conclude the following: If there is a dipolar modulation, then its amplitude must be running, i.e. $A(k)$ must be large on large scales and small on small scales. The consistency relation, Eq. (4.4), then implies that also f_{NL} must be running in the same way. There exists thus an interesting connection between the hemispherical power asymmetry and primordial non-Gaussianity.

To conclude, the hemispherical power asymmetry is certainly an interesting anomaly in the CMB sky, as it might give insight about inflation and primordial non-Gaussianity. However, the estimation of the statistical significance of CMB anomalies is in general problematic because of unquantified look-elsewhere effects and possible *a posteriori* statistics. Therefore, any anomaly can only be taken seriously if it can be explained within a theoretical model. If that model makes further predictions that can be tested, these can be used as further evidence for or against the model. For the hemispherical power asymmetry, several theoretical models do exist which explain its creation in the context of inflation. However, because no model so far has strong Bayesian support compared to ΛCDM, a final verdict in favour of this anomaly cannot be made at this point.

Chapter 5

Summary

In this thesis we have discussed some aspects of modern cosmology: the theory of structure formation, the concept of dark energy with particular focus on the integrated Sachs-Wolfe effect, and one interesting feature in the CMB sky, the hemispherical power asymmetry.

The theory of structure formation describes the transition of the early, homogeneous Universe to the inhomogeneous Universe we observe today, i.e. the formation of galaxies, clusters and superclusters. We have introduced a simple framework for this theory, which is based on perturbations described by Newtonian gravity on top of an expanding FRW universe. Within this framework, we were able to learn about the order of structure formation, which is a *bottom-up* evolution, i.e. small-scale structures form before large-scale structures. In order to match the theoretical linear matter power spectrum to observed galaxy power spectra, it is necessary to introduce a galaxy *bias*. Understanding the nonlinear formation of structure remains one of the biggest challenges of modern cosmology. We also discussed how the formation of structure is described in relativistic cosmological perturbation theory. We found a remarkable agreement between the Newtonian and relativistic descriptions on scales that are well within the horizon. However, on scales close to and larger than the horizon, we found differences between the two theories, in particular in the obtained linear matter power spectra.

Dark energy is not only the largest component, but certainly also one of the biggest mysteries of the Universe today. Although a cosmological constant Λ is the currently favoured explanation of cosmic acceleration, alternatives, such as quintessence models, modified gravity theories, or models based on an inhomogeneous metric, are not ruled out. Here, we have focused on a particular effect that is predicted by the presence of dark energy and which causes an imprint of the local large-scale structure into the CMB temperature anisotropies, the *integrated Sachs-Wolfe effect*. Due to its small amplitude, the ISW signal cannot be measured directly in the CMB, but it can be extracted by cross-correlation of the CMB with tracers of the local large-scale structure, e.g. galaxies. With the next generation of massive galaxy surveys, e.g. Euclid and the Dark Energy Survey, the significance of a detection of this effect will certainly improve, giving better constraints on

dark energy models. We also discussed an alternative approach to measure the ISW signal, which is based on stacking CMB patches along the lines of sight of the most extreme superstructures in the local large-scale structure. The result of such a measurement is however difficult to explain within the ΛCDM model.

The temperature anisotropies in the CMB encode a wealth of cosmological information. By studying the CMB, we can learn e.g. about inflation, the properties of the early Universe, as well as dark energy. The measured angular power spectrum of the CMB can be remarkably well described within the ΛCDM model. However, on the largest angular scales some features have been found that are unlikely to appear within the standard model, the CMB *anomalies*. These anomalies are certainly interesting as they might hint towards physics beyond the ΛCDM model, however estimating their statistical significance is difficult because of unquantified look-elsewhere effects and possible *a posteriori*-statistics in their detection. Here, we have focused on one particular anomaly which is based on an asymmetric distribution of power in the CMB sky, the *hemispherical power asymmetry*. This asymmetry is particularly interesting as it might give insight about the mechanics of cosmic inflation. In particular, it can be related to the existence of primordial non-Gaussianity in curvaton models.

Appendix

Perturbed Einstein tensor in longitudinal gauge

In the conformal Newtonian gauge, the metric tensor is

$$g_{\mu\nu} = a^2 \begin{pmatrix} -1 - 2\Phi & 0 \\ 0 & (1 - 2\Psi)\delta_{ij} \end{pmatrix},$$

and the inverse metric is

$$g^{\mu\nu} = a^{-2} \begin{pmatrix} -1 + 2\Phi & 0 \\ 0 & (1 + 2\Psi)\delta_{ij} \end{pmatrix}.$$

Given the metric tensor, we can construct the connection coefficients,

$$\Gamma^{\mu}_{\alpha\beta} \equiv \frac{1}{2} g^{\mu\lambda}(g_{\lambda\beta,\mu} + g_{\alpha\lambda,\beta} - g_{\alpha\beta,\lambda}).$$

In particular, we find

$$\Gamma^0_{00} = \mathcal{H} + \Phi', \qquad \Gamma^0_{0k} = \Phi_{,k}, \qquad \Gamma^0_{ij} = (\mathcal{H} - 2\mathcal{H}(\Phi + \Psi) + \Psi')\delta_{ij},$$
$$\Gamma^i_{00} = \Phi_{,i}, \qquad \Gamma^i_{0j} = (\mathcal{H} - \Psi')\delta_{ij}, \quad \Gamma^i_{kl} = -(\Psi_{,l}\delta^i_k + \Psi_{,k}\delta^i_l) + \Psi_{,i}\delta_{kl}.$$

The Ricci tensor is defined as

$$R_{\mu\nu} \equiv \Gamma^{\alpha}_{\mu\nu,\alpha} - \Gamma^{\alpha}_{\alpha\mu,\nu} + \Gamma^{\alpha}_{\alpha\beta}\Gamma^{\beta}_{\mu\nu} - \Gamma^{\alpha}_{\beta\mu}\Gamma^{\beta}_{\alpha\nu}.$$

The components are:

$$
\begin{aligned}
R_{00} &= -3\mathcal{H}' + 3\psi'' + \nabla^2\Phi + 3\mathcal{H}(\Phi' + \Psi'), \\
R_{0i} &= 2(\Psi' + \mathcal{H}\Phi)_{,i}, \\
R_{ij} &= (\mathcal{H}' + 2\mathcal{H}^2)\delta_{ij} \\
&\quad + [-\Psi'' + \nabla^2\Psi - \mathcal{H}(\Phi' + 5\Psi) - (2\mathcal{H}' + 4\mathcal{H}^2)(\Phi + \Psi)]\delta_{ij} \\
&\quad + (\Psi - \Phi)_{,ij}.
\end{aligned}
$$

Raising an index we find

$$
\begin{aligned}
R^0_0 &= 3a^{-2}\mathcal{H}' + a^{-2}[-3\psi'' - \nabla^2\Phi + -3\mathcal{H}(\Phi' + \Psi') - 6\mathcal{H}'\Phi], \\
R^0_i &= -2a^{-2}(\Psi' + \mathcal{H}\Phi)_{,i}, \\
R^i_0 &= 2a^{-2}(\Psi' + \mathcal{H}\Phi)_{,i}, \\
R^i_j &= a^{-2}(\mathcal{H}' + 2\mathcal{H}^2)\delta^i_j \\
&\quad + a^{-2}[-\Psi'' + \nabla^2\Psi - \mathcal{H}(\Phi' + 5\Psi) - (2\mathcal{H}' + 4\mathcal{H}^2)(\Phi + \Psi)]\delta_{ij} \\
&\quad + a^{-2}(\Psi - \Phi)_{,ij}.
\end{aligned}
$$

From this we find the Ricci scalar,

$$
\begin{aligned}
R &\equiv R^0_0 + R^i_i \\
&= 6a^{-2}(\mathcal{H}' + \mathcal{H}^2) \\
&\quad + a^{-2}[-6\Psi'' + 2\nabla^2(2\Psi - \Phi) - 6\mathcal{H}(\Phi' + 3\Psi') - 12(\mathcal{H}' + \mathcal{H}^2)\Phi].
\end{aligned}
$$

Finally, we can construct the Einstein tensor $G^\mu_\nu \equiv R^\mu_\nu - \frac{1}{2}R\delta^\mu_\nu$,

$$
\begin{aligned}
G^0_0 &= -3a^{-2}\mathcal{H}^2 + a^{-2}[2\nabla^2\Psi + 6\mathcal{H}\Psi' + 6\mathcal{H}^2\Phi], \\
G^0_i &= R^0_i = -2a^{-2}(\Psi' + \mathcal{H}\Phi)_{,i}, \\
G^i_0 &= R^i_0 = 2a^{-2}(\Psi' + \mathcal{H}\Phi)_{,i}, \\
G^i_j &= R^i_j - \frac{1}{2}R\delta^i_j \\
&= a^{-2}(-2\mathcal{H}' - \mathcal{H}^2)\delta^i_j \\
&\quad + a^{-2}[2\Psi'' + \nabla^2(\Phi - \Psi) + \mathcal{H}(2\Phi' + 4\Psi') + (4\mathcal{H}' + 2\mathcal{H}^2)\Phi]\delta^i_j \\
&\quad + a^{-2}(\Psi - \Phi)_{,ij}.
\end{aligned}
$$

References

[1] S. F. Flender and D. J. Schwarz, *Newtonian versus relativistic cosmology*, *Phys.Rev.* **D86** (2012) 063527, [arXiv:1207.2035].

[2] S. Flender, S. Hotchkiss, and S. Nadathur, *The stacked ISW signal of rare superstructures in ΛCDM*, *JCAP* **1302** (2013) 013, [arXiv:1212.0776].

[3] S. Flender and S. Hotchkiss, *The small scale power asymmetry in the cosmic microwave background*, *JCAP* **1309** (2013) 033, [arXiv:1307.6069].

[4] Planck Collaboration, P. Ade *et. al.*, *Planck 2013 results. XVI. Cosmological parameters*, arXiv:1303.5076.

[5] I. Gott, J. Richard, M. Juric, D. Schlegel, F. Hoyle, M. Vogeley, *et. al.*, *A map of the universe*, *Astrophys.J.* **624** (2005) 463, [astro-ph/0310571].

[6] A.H. Liddle and D.H. Lyth, *Cosmological Inflation and Large-Scale Structure*, Cambridge University Press 2000.

[7] G. Bertone, D. Hooper, and J. Silk, *Particle dark matter: Evidence, candidates and constraints*, *Phys.Rept.* **405** (2005) 279–390, [hep-ph/0404175].

[8] D. H. Weinberg, M. J. Mortonson, D. J. Eisenstein, C. Hirata, A. G. Riess, *et. al.*, *Observational Probes of Cosmic Acceleration*, *Phys.Rept.* **530** (2013) 87–255, [arXiv:1201.2434].

[9] V.F. Mukhanov, *Physical Foundations of Cosmology*, Cambridge University Press 2005.

[10] R. M. Wald, *General Relativity*, Chicago, Usa: Univ. Pr. (1984).

[11] S. M. Carroll, *Spacetime and Geometry: An Introduction to General Relativity*, San Francisco, USA: Addison-Wesley (2004).

[12] C. Frenk and S. D. White, *Dark matter and cosmic structure*, *Annalen Phys.* **524** (2012) 507–534, [arXiv:1210.0544].

[13] D. Fixsen, *The Temperature of the Cosmic Microwave Background*, *Astrophys.J.* **707** (2009) 916–920, [arXiv:0911.1955].

[14] M. Hindmarsh and T. Kibble, *Cosmic strings*, *Rept.Prog.Phys.* **58** (1995) 477–562, [`hep-ph/9411342`].

[15] Planck Collaboration, P. Ade *et. al.*, *Planck 2013 results. I. Overview of products and scientific results*, `arXiv:1303.5062`.

[16] J. Valiviita, *The Nature of Primordial Perturbations in the Light of CMB Observations*, Doctoral Disseration, University of Helsinki 2005.

[17] R. Sachs and A. Wolfe, *Perturbations of a cosmological model and angular variations of the microwave background*, *Astrophys.J.* **147** (1967) 73–90.

[18] E. Bertschinger, *Cosmological dynamics: Course 1*, `astro-ph/9503125`.

[19] V. Mukhanov, *Quantum Cosmological Perturbations: Predictions and Observations*, *Eur.Phys.J.* **C73** (2013) 2486, [`arXiv:1303.3925`].

[20] J. M. Bardeen, *Cosmological perturbations: From quantum fluctuations to large scale structure*, Lectures given at 2nd Guo Shou-jing Summer School on Particle Physics and Cosmology, Nanjing, China, Jul 1988.

[21] J. M. Bardeen, J. Bond, N. Kaiser, and A. Szalay, *The Statistics of Peaks of Gaussian Random Fields*, *Astrophys.J.* **304** (1986) 15–61.

[22] C. Knobel, *An introduction into the theory of cosmological structure formation*, `arXiv:1208.5931`.

[23] J. Peacock and R. Smith, *Halo occupation numbers and galaxy bias*, *Mon.Not.Roy.Astron.Soc.* **318** (2000) 1144, [`astro-ph/0005010`].

[24] S. D. M. White and M. Rees, *Core condensation in heavy halos: A Two stage theory for galaxy formation and clusters*, *Mon.Not.Roy.Astron.Soc.* **183** (1978) 341–358.

[25] S. Finkelstein *et. al.*, *A galaxy rapidly forming stars 700 million years after the Big Bang at redshift 7.51*, *Nature* **502**.

[26] `http://ned.ipac.caltech.edu/level5/Sept03/Peacock/Peacock6_2.html`.

[27] SDSS Collaboration, M. Tegmark *et. al.*, *Cosmological Constraints from the SDSS Luminous Red Galaxies*, *Phys.Rev.* **D74** (2006) 123507, [`astro-ph/0608632`].

[28] N. Kaiser, *On the Spatial correlations of Abell clusters*, *Astrophys.J.* **284** (1984) L9–L12.

[29] M. Tegmark and P. Peebles, *The Time evolution of bias*, *Astrophys.J.Lett.* (1998) [`astro-ph/9804067`].

[30] V. F. Mukhanov, H. Feldman, and R. H. Brandenberger, *Theory of cosmological perturbations. Part 1. Classical perturbations. Part 2. Quantum theory of perturbations. Part 3. Extensions*, *Phys.Rept.* **215** (1992) 203–333.

[31] H. Kurki-Suonio, *Cosmological Perturbation Theory* (lecture notes), University of Helsinki 2010.

[32] J. M. Bardeen, *Gauge Invariant Cosmological Perturbations*, *Phys.Rev.* **D22** (1980) 1882–1905.

[33] N. E. Chisari and M. Zaldarriaga, *Connection between Newtonian simulations and general relativity*, *Phys.Rev.* **D83** (2011) 123505, [`arXiv:1101.3555`].

[34] S. R. Green and R. M. Wald, *Newtonian and Relativistic Cosmologies*, *Phys.Rev.* **D85** (2012) 063512, [`arXiv:1111.2997`].

[35] J. Adamek, D. Daverio, R. Durrer, and M. Kunz, *General Relativistic N-body simulations in the weak field limit*, *Phys.Rev.* **D88** (2013) 103527, [`arXiv:1308.6524`].

[36] J. Yoo, A. L. Fitzpatrick, and M. Zaldarriaga, *A New Perspective on Galaxy Clustering as a Cosmological Probe: General Relativistic Effects*, *Phys.Rev.* **D80** (2009) 083514, [`arXiv:0907.0707`].

[37] J. Yoo, *General Relativistic Description of the Observed Galaxy Power Spectrum: Do We Understand What We Measure?*, *Phys.Rev.* **D82** (2010) 083508, [`arXiv:1009.3021`].

[38] C. Bonvin and R. Durrer, *What galaxy surveys really measure*, *Phys.Rev.* **D84** (2011) 063505, [`arXiv:1105.5280`].

[39] A. Challinor and A. Lewis, *The linear power spectrum of observed source number counts*, *Phys.Rev.* **D84** (2011) 043516, [`arXiv:1105.5292`].

[40] S. Maddox, G. Efstathiou, W. Sutherland, and J. Loveday, *Galaxy correlations on large scales*, *Mon.Not.Roy.Astron.Soc.* **242** (1990) 43–49.

[41] G. Efstathiou, W. Sutherland, and S. Maddox, *The cosmological constant and cold dark matter*, *Nature* **348** (1990) 705–707.

[42] S. Cole, D. H. Weinberg, C. S. Frenk, and B. Ratra, *Large scale structure in COBE normalized cold dark matter cosmogonies*, *Mon.Not.Roy.Astron.Soc.* **289** (1997) 37, [`astro-ph/9702082`].

[43] M. Pierce, D. Welch, R. McClure, S. van den Bergh, R. Racine, *et. al.*, *The Hubble constant and Virgo cluster distance from observations of Cepheid variables*, *Nature* **371** (1994) 385–389.

[44] B. Chaboyer, P. J. Kernan, L. M. Krauss, and P. Demarque, *A Lower limit on the age of the universe*, *Science* **271** (1996) 957–961, [`astro-ph/9509115`].

[45] M. Phillips, *The absolute magnitudes of Type IA supernovae*, *Astrophys.J.* **413** (1993) L105–L108.

[46] A. G. Riess, W. H. Press, and R. P. Kirshner, *A Precise distance indicator: Type Ia supernova multicolor light curve shapes*, Astrophys.J. **473** (1996) 88, [`astro-ph/9604143`].

[47] Supernova Search Team, A. G. Riess *et. al.*, *Observational evidence from supernovae for an accelerating universe and a cosmological constant*, Astron.J. **116** (1998) 1009–1038, [`astro-ph/9805201`].

[48] Supernova Cosmology Project, S. Perlmutter *et. al.*, *Measurements of Omega and Lambda from 42 high redshift supernovae*, Astrophys.J. **517** (1999) 565–586, [`astro-ph/9812133`].

[49] Boomerang Collaboration, P. de Bernardis *et. al.*, *A Flat universe from high resolution maps of the cosmic microwave background radiation*, Nature **404** (2000) 955–959, [`astro-ph/0004404`].

[50] S. Hanany, P. Ade, A. Balbi, J. Bock, J. Borrill, *et. al.*, *MAXIMA-1: A Measurement of the cosmic microwave background anisotropy on angular scales of 10 arcminutes to 5 degrees*, Astrophys.J. **545** (2000) L5, [`astro-ph/0005123`].

[51] M. Peskin and D. Schroeder, *An Introduction to quantum field theory*, Westview Press 1995.

[52] R. R. Caldwell, M. Kamionkowski, and N. N. Weinberg, *Phantom energy and cosmic doomsday*, Phys.Rev.Lett. **91** (2003) 071301, [`astro-ph/0302506`].

[53] T. S. Koivisto, *Formation of Structure in Dark Energy Cosmologies*, Doctoral Disseration, University of Helsinki 2006.

[54] M. Li, X.-D. Li, S. Wang, and Y. Wang, *Dark Energy: a Brief Review*, `arXiv:1209.0922`.

[55] O. Gron, *A new standard model of the universe*, Eur.J.Phys. **23** (2002) 135–144, [`arXiv:0801.0552`].

[56] M. Rees and D. Sciama, *Large scale Density Inhomogeneities in the Universe*, Nature **217** (1968) 511–516.

[57] Y.-C. Cai, S. Cole, A. Jenkins, and C. S. Frenk, *Full-sky map of the ISW and Rees-Sciama effect from Gpc simulations*, `arXiv:1003.0974`.

[58] R. G. Crittenden and N. Turok, *Looking for Lambda with the Rees-Sciama effect*, Phys.Rev.Lett. **76** (1996) 575, [`astro-ph/9510072`].

[59] T. Giannantonio, R. Crittenden, R. Nichol, and A. J. Ross, *The significance of the integrated Sachs-Wolfe effect revisited*, Mon.Not.Roy.Astron.Soc. **426** (2012) 2581–2599, [`arXiv:1209.2125`].

[60] F.-X. Dupe, A. Rassat, J.-L. Starck, and M. Fadili, *Measuring the Integrated Sachs-Wolfe Effect*, `arXiv:1010.2192`.

[61] Planck Collaboration, P. Ade *et. al.*, *Planck 2013 results. XIX. The integrated Sachs-Wolfe effect*, `arXiv:1303.5079`.

[62] B. R. Granett, M. C. Neyrinck, and I. Szapudi, *An Imprint of Super-Structures on the Microwave Background due to the Integrated Sachs-Wolfe Effect*, `arXiv:0805.3695`.

[63] P. Hunt and S. Sarkar, *Constraints on large scale inhomogeneities from WMAP-5 and SDSS: confrontation with recent observations*, *Mon.Not.Roy.Astron.Soc.* **401** (2010) 547, [`arXiv:0807.4508`].

[64] S. Nadathur, S. Hotchkiss, and S. Sarkar, *The integrated Sachs-Wolfe imprints of cosmic superstructures: a problem for ΛCDM*, *JCAP* **1206** (2012) 042, [`arXiv:1109.4126`].

[65] C. Hernandez-Monteagudo and R. E. Smith, *On the signature of nearby superclusters and voids in the Integrated Sachs-Wolfe effect*, `arXiv:1212.1174`.

[66] D. Schwarz, G. Starkman, D. Huterer, and C. Copi, *Is the Low-l Microwave Background cosmic?*, *Phys.Rev.Lett.* **93** (2004) 221301.

[67] C. Bennett, R. Hill, G. Hinshaw, D. Larson, K. Smith, *et. al.*, *Seven-Year Wilkinson Microwave Anisotropy Probe (WMAP) Observations: Are There Cosmic Microwave Background Anomalies?*, *Astrophys.J.Suppl.* **192** (2011) 17, [`arXiv:1001.4758`].

[68] Planck Collaboration, P. Ade *et. al.*, *Planck 2013 results. XXIII. Isotropy and Statistics of the CMB*, `arXiv:1303.5083`.

[69] CMS Collaboration, S. Chatrchyan *et. al.*, *Observation of a new boson at a mass of 125 GeV with the CMS experiment at the LHC*, *Phys.Lett.* **B716** (2012) 30–61, [`arXiv:1207.7235`].

[70] ATLAS Collaboration, G. Aad *et. al.*, *Observation of a new particle in the search for the Standard Model Higgs boson with the ATLAS detector at the LHC*, *Phys.Lett.* **B716** (2012) 1–29, [`arXiv:1207.7214`].

[71] H. Jeffreys, Theory of probability, 3rd edn , Oxford Classics series (reprinted 1998) (Oxford University Press, Oxford, UK, 1961).

[72] R. Trotta, *Bayes in the sky: Bayesian inference and model selection in cosmology*, *Contemp.Phys.* **49** (2008) 71–104, [`arXiv:0803.4089`].

[73] F. Hansen, A. Banday, K. Gorski, H. Eriksen, and P. Lilje, *Power Asymmetry in Cosmic Microwave Background Fluctuations from Full Sky to Sub-degree Scales: Is the Universe Isotropic?*, *Astrophys.J.* **704** (2009) 1448–1458, [`arXiv:0812.3795`].

[74] H. Eriksen, F. Hansen, A. Banday, K. Gorski, and P. Lilje, *Asymmetries in the Cosmic Microwave Background anisotropy field*, *Astrophys.J.* **605** (2004) 14–20, [`astro-ph/0307507`].

[75] F. K. Hansen, A. Banday, and K. Gorski, *Testing the cosmological principle of isotropy: Local power spectrum estimates of the WMAP data*, *Mon.Not.Roy.Astron.Soc.* **354** (2004) 641–665, [`astro-ph/0404206`].

[76] C. Gordon, W. Hu, D. Huterer, and T. M. Crawford, *Spontaneous isotropy breaking: a mechanism for cmb multipole alignments*, *Phys.Rev.* **D72** (2005) 103002, [`astro-ph/0509301`].

[77] H. K. Eriksen, A. Banday, K. Gorski, F. Hansen, and P. Lilje, *Hemispherical power asymmetry in the three-year Wilkinson Microwave Anisotropy Probe sky maps*, *Astrophys.J.* **660** (2007) L81–L84, [`astro-ph/0701089`].

[78] J. Hoftuft, H. Eriksen, A. Banday, K. Gorski, F. Hansen, *et. al.*, *Increasing evidence for hemispherical power asymmetry in the five-year WMAP data*, *Astrophys.J.* **699** (2009) 985–989, [`arXiv:0903.1229`].

[79] C. Gordon and R. Trotta, *Bayesian Calibrated Significance Levels Applied to the Spectral Tilt and Hemispherical Asymmetry*, *Mon.Not.Roy.Astron.Soc.* **382** (2007) 1859–1863, [`arXiv:0706.3014`].

[80] A. L. Erickcek, M. Kamionkowski, and S. M. Carroll, *A Hemispherical Power Asymmetry from Inflation*, *Phys.Rev.* **D78** (2008) 123520, [`arXiv:0806.0377`].

[81] C. Gordon, *Broken Isotropy from a Linear Modulation of the Primordial Perturbations*, *Astrophys.J.* **656** (2007) 636–640, [`astro-ph/0607423`].

[82] A. Mazumdar and L. Wang, *CMB dipole asymmetry from a fast roll phase*, `arXiv:1306.5736`.

[83] D. H. Lyth, *The CMB asymmetry from inflation*, `arXiv:1304.1270`.

[84] K. Enqvist and M. S. Sloth, *Adiabatic CMB perturbations in pre - big bang string cosmology*, *Nucl.Phys.* **B626** (2002) 395–409, [`hep-ph/0109214`].

[85] T. Moroi and T. Takahashi, *Effects of cosmological moduli fields on cosmic microwave background*, *Phys.Lett.* **B522** (2001) 215–221, [`hep-ph/0110096`].

[86] D. H. Lyth and D. Wands, *Generating the curvature perturbation without an inflaton*, *Phys.Lett.* **B524** (2002) 5–14, [`hep-ph/0110002`].

[87] C. M. Hirata, *Constraints on cosmic hemispherical power anomalies from quasars*, *JCAP* **0909** (2009) 011, [`arXiv:0907.0703`].